Cell Reports

Article

Redox proteomics reveal a role for peroxiredoxinylation in stress protection

Graphical abstract

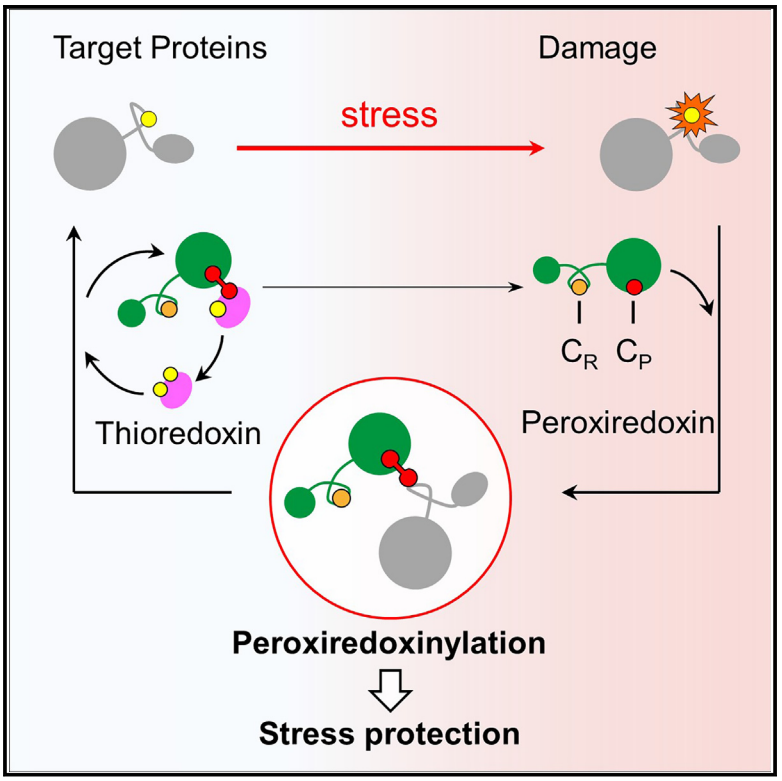

Authors

Gerhard Seisenbacher, Zrinka Raguz Nakic, Eva Borràs, Eduard Sabidó, Uwe Sauer, Eulalia de Nadal, Francesc Posas

Correspondence

eulalia.nadal@irbbarcelona.org (E.d.N.), francesc.posas@irbbarcelona.org (F.P.)

In brief

In redox signaling, peroxiredoxins are key regulators modulating cysteine oxidation on target proteins. Here, Seisenbacher et al. report a redox-sensitive interactome of the *S. cerevisiae* peroxiredoxin Tsa1 and show that the covalent attachment of Tsa1 to target proteins protects cellular processes and contributes to survival upon environmental stress.

Highlights

- The peroxiredoxin Tsa1 interacts with a large fraction of the proteome in a redox manner
- Covalent Tsa1 attachment to target proteins (peroxiredoxinylation) increases upon stress
- Metabolic enzymes and proteins involved in translation are targeted by Tsa1
- Stress survival requires peroxiredoxinylation of the 6-phosphogluconate dehydrogenase

Seisenbacher et al., 2025, Cell Reports *44*, 115224
February 25, 2025
https://doi.org/10.1016/j.celrep.2024.115224

CellPress

Cell Reports

CellPress
OPEN ACCESS

Article

Redox proteomics reveal a role for peroxiredoxinylation in stress protection

Gerhard Seisenbacher,[1,2] Zrinka Raguz Nakic,[3,4] Eva Borràs,[1,5] Eduard Sabidó,[1,5] Uwe Sauer,[3] Eulalia de Nadal,[1,2,*] and Francesc Posas[1,2,6,*]

[1]Department of Medicine and Life Sciences, Universitat Pompeu Fabra, 08003 Barcelona, Spain
[2]Institute for Research in Biomedicine (IRB Barcelona), Barcelona Institute of Science and Technology, 08028 Barcelona, Spain
[3]Institute of Molecular Systems Biology, ETH Zürich, 8093 Zurich, Switzerland
[4]ZHAW School of Life Sciences and Facility Management, Biosystems Technology, 8820 Wädenswil, Switzerland
[5]Centre of Genomic Regulation, Barcelona Institute of Science and Technology, 08003 Barcelona, Spain
[6]Lead contact
*Correspondence: eulalia.nadal@irbbarcelona.org (E.d.N.), francesc.posas@irbbarcelona.org (F.P.)
https://doi.org/10.1016/j.celrep.2024.115224

SUMMARY

The redox state of proteins is essential for their function and guarantees cell fitness. Peroxiredoxins protect cells against oxidative stress, maintain redox homeostasis, act as chaperones, and transmit hydrogen peroxide signals to redox regulators. Despite the profound structural and functional knowledge of peroxiredoxins action, information on how the different functions are concerted is still scarce. Using global proteomic analyses, we show here that the yeast peroxiredoxin Tsa1 interacts with many proteins of essential biological processes, including protein turnover and carbohydrate metabolism. Several of these interactions are of a covalent nature, and we show that failure of peroxiredoxinylation of Gnd1 affects its phosphogluconate dehydrogenase activity and impairs recovery upon stress. Thioredoxins directly remove TSA1-formed mixed disulfide intermediates, thus expanding the role of the thioredoxin-peroxiredoxin redox cycle pair to buffer the redox state of proteins.

INTRODUCTION

Regulation of redox modifications is essential for protein function and to guarantee cell fitness.[1] Peroxiredoxins (PRXs), found in all domains of life, arose as central players in the antioxidant response. Despite moderate peroxidase activity, their abundance enables them to detoxify up to 90% of cytosolic H_2O_2.[2] PRXs are essential in redox processes ranging from oxidative stress protection to redox signaling.[3] Disruption of peroxiredoxin function results in decreased cell fitness and is linked to aging, inflammation, neurological diseases, and cancer.[4] 2-Cys PRXs rely on a peroxidatic cysteine (C_P) that reacts with peroxides and a resolving cysteine (C_R) to react with the sulfenic C_P and to drive the catalytic redox cycle.[5]

Oxidative protein modifications, initially considered primarily damaging, are now recognized as physiologically important.[6] The role of H_2O_2 as a second messenger is well established, and thiol oxidations have been added to a list of cysteine post-translational modifications such as glutathionylation, sulfhydrylation, and nitrosation.[7–9] For instance, the ATPase alpha subunit has a redox-modified cysteine (C294) that directly affects ATP production.[10] Glutathionylation of Cys374 of actin enhances depolymerization and plays a role in stress fiber formation.[11,12] Transient glutathionylation of glycerol aldehyde-3-phosphate dehydrogenase protects its enzymatic site from irreversible oxidation during oxidative stress.[13]

The functional dissection of the peroxidatic cysteine was key to understanding H_2O_2 as a second messenger. The central PXXX(S/T)XXC_P motif is highly conserved, but the molecular environment changed to favor the C_P hyperoxidation in eukaryotes compared to bacteria.[14] This oxidative inactivation allows H_2O_2 levels to rise and act as a redox signaling messenger.[7,8,15–17] Another consequence of the C_P sulfonic acid form is the formation of higher-order structures with a chaperone function.[18] In contrast, the majority of cysteine thiol groups found in proteins have moderate reactivity toward low, physiological H_2O_2 concentrations. In this context, PRXs function as mediators of redox signaling.[19–21] The oxidized peroxidatic cysteine forms transient mixed disulfide intermediates (MDIs) with a target protein thiol, and a disulfide exchange reaction with a vicinal cysteine in the target leads to a disulfide bridge-modified protein, transmitting the cellular redox state to regulatory proteins such as Stat3 or Bcy1.[19–21] Recently, it has been shown that association of the PRX Tpx1 with Sty1 leads to the formation of a signaling complex that activates stress-activated protein kinase signaling independent of the canonical activation pathway in *S. pombe*.[22] Thus, redox-sensitive PRX-protein interactions are potentially widespread, and novel modes of action are likely to be discovered. Correspondingly, large-scale proteomics experiments in eukaryotic organisms revealed the extended formation of MDIs by PRXs.[23,24] However, how PRXs select their targets or how the formation of adventitious mixed disulfides is prevented is not well understood.[21,23,25]

The highly expressed PRX *TSA1* from *S. cerevisiae* has been pivotal in the structural and functional understanding of eukaryotic 2-Cys PRX.[20,26–28] Here, we show, using global proteomic analyses, that Tsa1 physically interacts with hundreds of

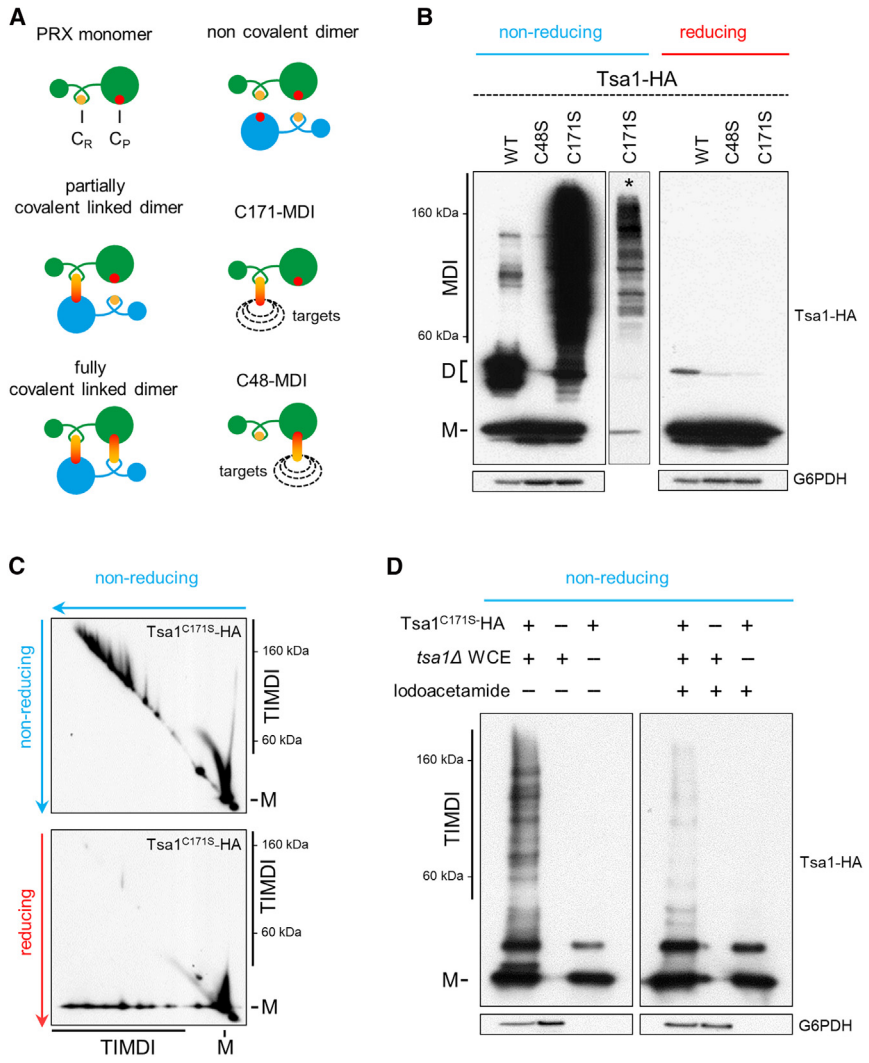

Figure 1. Tsa1 forms widespread covalent association relying on its peroxidatic cysteine

(A) Covalent cysteine interactions of 2-Cys peroxiredoxins (PRXs). C_P and C_R indicate the peroxidatic and resolving cysteine, respectively. Mixed disulfide intermediates of targets (dashed black circles). Evidence for the dimeric forms is in Figure S1E.

(B) Detection of mixed disulfide intermediates (MDIs) by reducing and non-reducing (NR) western blot. Lower exposure (*) of the Tsa1^{C171S}-HA lane. Shorter exposures and experiments with untagged Tsa1 are in Figure S1D.

(C) The redox-sensitive presence of Tsa1^{C171S}-HA in the high-molecular-weight (HMW) adducts is confirmed by 2D SDS-PAGE western blots. Experimental outline is found in Figure S1F.

(D) *In vitro* Tsa1-induced mixed disulfide intermediate (TIMDI) formation. *tsa1Δ* whole-cell extracts were incubated with recombinant Tsa1^{C171S}-HA. Iodoacetamide was used as a free thiol blocker.

D, fully and partially disulfide-linked Tsa1 homodimer; M, Tsa1 monomer; MDI/TIMDI, mixed disulfide intermediates.

proteins of central biological processes. Interestingly, the majority of those interactions is redox sensitive, and several are covalent by the formation of disulfide bridges involving the peroxidatic cysteine and cysteines in the target protein. Remarkably, this binding is independent of its hyperoxidized chaperone function and independent of the recently described mechanism during oxidative aging involving sulfiredoxin and the Hsp70/Hsp104 heat shock protein complex.[29] Instead, we find that the covalent interaction of PRXs with its interactome is induced by various stresses and is regulated by the thioredoxin system, thus indicating a role for the association of Tsa1 in protecting the redox state of the proteome upon cellular stress.

RESULTS

Tsa1 forms widespread MDIs

MDIs of PRXs are the base of redox relays that are widely found in eukaryotes.[24,30,31] Similar to observations in mammalian cells, we suspected that important functions of the yeast PRX Tsa1 could be mediated by MDIs.[21,23] Therefore, we tested wild-type (WT), the peroxidatic cysteine (C48S), and the resolving cysteine (C171S) mutants of Tsa1 for their ability to form MDIs and distinguish the importance of the respective cysteines in their formation (Figure 1A). Importantly, the single C-terminal hemagglutinin (HA) epitope in the endogenous locus does not affect Tsa1 expression or function (Figures S1A–S1C). Under non-reducing (NR) conditions, HA-tagged and untagged WT Tsa1 form MDIs in the 50- to 200-kDa range, referred to herein as Tsa1-induced MDIs (TIMDIs) (Figure 1B, S1D, and S1E). TIMDIs are strongly enhanced in the C171S mutant and absent in the C48S mutant (Figures 1B and S1D). The denaturing base of SDS-PAGE confirms the covalent nature of these adducts, and their absence in reducing conditions indicates the redox sensitivity of the potential Tsa1-target protein attachment. Both the peroxidatic and resolving mutant display redox cycle defects but exhibit opposing phenotypes in TIMDI formation. To prove that the high-molecular-weight (HMW) TIMDIs contain Tsa1, we performed a two-dimensional SDS-PAGE, as outlined in Figure S1F. The collapse of the Tsa1^{C171S}-HA TIMDIs to monomeric Tsa1 in reducing conditions confirmed the association of Tsa1 with target proteins of various molecular weights (Figure 1C). Additionally, TIMDI formation could be recapitulated *in vitro* using *Δtsa1* whole-cell extract and Tsa1^{C171S}-HA. Correspondingly, blocking free cysteines strongly reduces TIMDI formation (Figure 1D). Thus, Tsa1 has the potential to form covalent disulfide bridges via its peroxidatic cysteine with its targets. Rapid intramolecular disulfide exchange by a structurally close cysteine makes MDIs transient, releasing a reduced PRX and an oxidized target

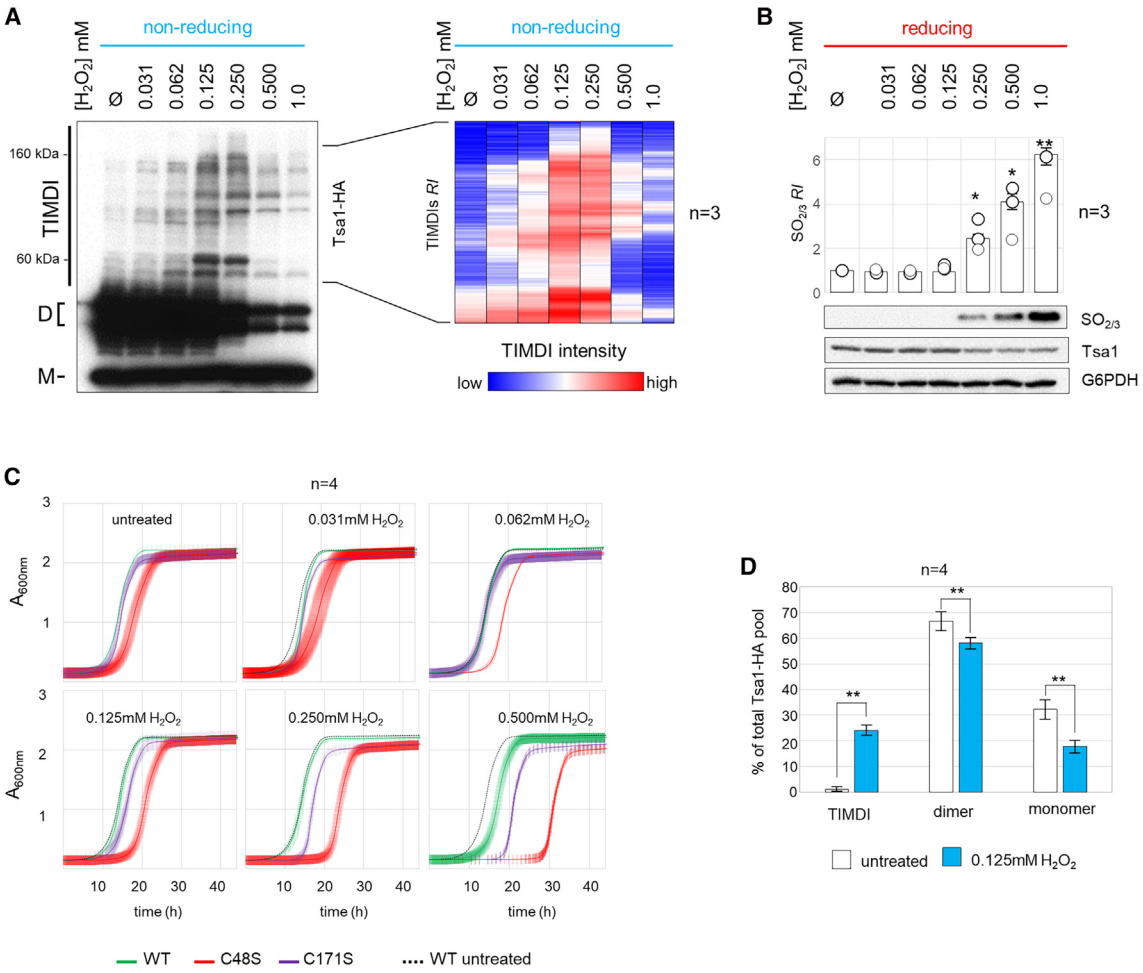

Figure 2. Tsa1-induced mixed disulfide increases in a dose response to H_2O_2

(A) Tsa1^{WT}-HA cultures were treated with the indicated H_2O_2 concentration for 10 min, and TIMDI induction was analyzed by western blot. Lower exposures and change in the Tsa1 monomer:homodimer ratio are in Figure S2A. Relative TIMDI intensities (*RI*) are shown as heatmaps ($n = 3$). Log_2-fold change and statistical analysis are in Figure S2B.

(B) Western blot analysis of cysteine sulfinylation/sulfonylation ($SO_{2/3}$) of H_2O_2 dose response (A). Relative $SO_{2/3}$ intensities (*RI*) ($n = 3$), median values ± SDs and single data points (circles). Two-tailed Student's t test; $^*p < 0.05$; $^{**}p < 0.005$.

(C) Growth curves of the indicated strains upon H_2O_2 stress ($n = 4$). The unstressed Tsa1^{WT}-HA curve (dashed black line) is depicted in each graph for comparison. Median values ± SDs are shown.

(D) Percentages of TIMDIs, monomer, and dimer of the Tsa1^{WT}-HA in unstressed and H_2O_2-treated conditions determined by western blot quantification ($n = 4$). Two-tailed Student's t test; $^{**}p < 0.005$. Linear range estimation for quantification can be found in Figure S2E.

protein. This mechanism would also apply to C171S-MDIs, and therefore an increase in oxidized target proteins would be expected instead of in PRX-target MDIs. However, the extent of TIMDIs in Tsa1^{C171S}-HA suggests covalent attachment via the peroxidatic cysteine could act as a post-translational cysteine modification.[9]

TIMDIs are induced upon H_2O_2 stress

In mammals, 2-Cys PRXs have been established as forwarders of H_2O_2-derived oxidizing equivalents in protein thiol oxidation and redox signaling.[21,23] Given the low TIMDI levels of WT Tsa1 under unstressed conditions, we tested whether H_2O_2 stimulation induced TIMDIs. We followed TIMDI induction of Tsa1^{WT}-HA in a 10-min H_2O_2 dose response *in vivo* (newly synthesized antioxidants; e.g., catalases do not matter yet, and concentrations higher than 1 mM are considered severe oxidative stress[32–34]). At physiological H_2O_2 concentrations (0.031–0.062 mM), TIMDIs increased slightly. A significant burst occurred at levels permissive for redox signaling (0.125–0.25 mM), without causing substantial Tsa1 peroxidatic cysteine hyperoxidation (C48-$SO_{2/3}$) or lethality (Figures 2A–2C and S2A).[35] At higher H_2O_2 levels, which affect fitness and lead to irreversible peroxidatic cysteine oxidation, the formation of TIMDIs was prevented (Figures 2A–2C, S2A, and S2B). To confirm that TIMDIs are not artifacts, we assessed untagged Tsa1 under H_2O_2 dose response and compared thiol-blocking agents, finding similar results (Figures S2C–S2E).

For quantitative estimation, we measured TIMDIs and Tsa1 homo-dimer and monomer levels by analyzing Tsa1^{WT}-HA lanes

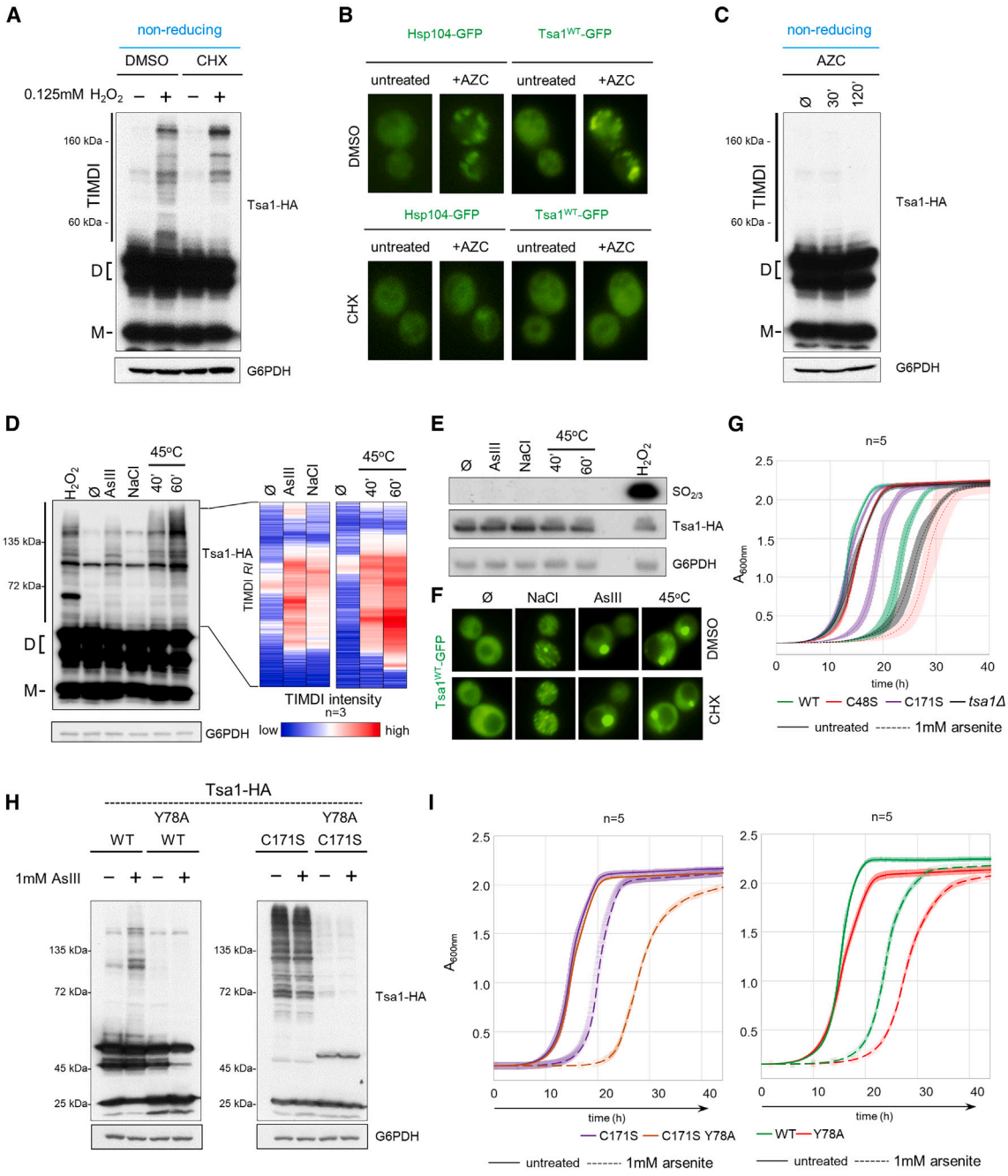

Figure 3. TIMDIs are induced upon environmental stress, protect against arsenite toxicity, and are independent of *de novo* protein production

(A) *De novo* protein production and TIMDI formation. Cells were pretreated with 100 μg/mL cyclohexamide for 15 min followed by ±1 mM H_2O_2 for 10 min.

(B) Aggregation of *de novo* proteins by L-azetidine-2-carboxylic acid treatment (AZC). Cycloheximide-sensitive foci formation of Hsp104-GFP and Tsa1-GFP were recorded 60 min after 5-mM AZC treatment. See Figure S3A for untreated controls.

(C) Protein aggregation does not induce TIMDIs. Tsa1^{WT}-HA cells were treated with 5 mM AZC for the indicated time points.

(D) NR whole-cell extracts of Tsa1^{WT}-HA strains treated with the indicated stresses were analyzed by western blot. Relative TIMDI intensities (*RI*) are shown as heatmaps (n = 3). Log_2-fold change and statistical analysis are in Figure S3C. Concentration and heat shock intensity estimation are in Figure S3B.

(E) C48-$SO_{2/3}$ of Tsa1-HA was assessed for the indicated stresses and compared to 1 mM H_2O_2 by western blot.

(F) Tsa1-GFP foci formation at the indicated stresses. DMSO or chlorhexidine pretreatment for 15 min. Hsp104-GFP foci formation is displayed in Figure S3D.

(legend continued on next page)

in a linear range on western blot (Figures S2F). H_2O_2 stress increased TIMDIs from barely detectible to over 20% of the Tsa1 pool (Figure 2D). As one of the most highly expressed proteins, the extent of TIMDI formation during oxidative stress is likely physiologically relevant. In contrast, the paralog Tsa2, expressed at much lower levels, does not appear to contribute significantly to TIMDI formation (Figure S2G).[36]

TIMDIs protect against protein damage upon stress

Tsa1 acts as a ribosome-associated chaperone to protect newly synthesized proteins and prevent protein aggregation upon oxidative stress.[20,26,37,38] We tested whether TIMDI formation arises from errors in *de novo* protein synthesis. Translation block by cycloheximide did not prevent TIMDIs in cells treated with 0.125 mM H_2O_2 (Figure 3A). AZC (L-azetidine-2-carboxylic acid), which causes misfolded protein accumulation, induced Tsa1-GFP and Hsp104-GFP foci, indicating co-translational aggregation (Figure 3B and S3A).[39] However, AZC did not induce TIMDIs (Figure 3C). Thus, TIMDI formation takes place at moderate H_2O_2 levels that do not saturate the PRX system and do not rely on *de novo* protein production.

Other stresses (arsenite, sodium chloride, and heat) that affect protein homeostasis and the cellular redox balance lead to the formation of TIMDIs (Figure 3D, S3B, and S3C).[40–43] Notably, these stresses did not cause Tsa1 hyperoxidation, differentiating TIMDI formation from hyperoxidized Tsa1 chaperone activity (Figure 3E). Arsenite, osmotic, and heat stress induced Tsa1-GFP foci that were not affected by cycloheximide (Figure 3F). While Hsp104-GFP foci behaved similarly upon osmostress, heat and arsenite stress-induced foci appear more dispersed and were considerably affected by cycloheximide (Figure S3D). Thus, the cycloheximide-sensitive phenotype indicates a qualitative difference, with Hsp104 being involved in *de novo* protein protection and Tsa1 acting on mature proteins in the tested stress situations.

Arsenite, an important environmental toxic pollutant, strongly induces TIMDIs.[44] The sodium arsenite tolerance correlated with TIMDI formation; the *tsa1Δ* deletion and $Tsa1^{C48S}$-HA strains were more sensitive to arsenite, while the $Tsa1^{C171S}$-HA mutant grew better, linking TIMDIs to stress adaptation (Figure 3G). Introducing a Y78A mutation prevents TIMDIs, in $Tsa1^{WT}$-HA and $Tsa1^{C171S}$-HA, in basal conditions and arsenite stress[45] (Figure 3H). Importantly, the Y78A mutation reversed the arsenite resistance of $Tsa1^{C171S}$-HA and increased the arsenite sensitivity of $Tsa1^{WT}$-HA, with no impact on survival under unstressed conditions (Figure 3I).

Human Prdx2 can act as a glutathione (GSH) peroxidase, and glutathionylation is protective during H_2O_2 stress.[13,46] We explored protein glutathionylation in H_2O_2 and arsenite stress (Figures S3E and S3F). Except for a prominent signal that corresponds to Tdh3 upon H_2O_2 stress, we did not observe any marked protein glutathionylation (Figure S3F). Tdh3 glutathionylation and Hsp104 expression is higher in the Tsa1 C48S mutant, indicative of an increased basal oxidative stress state (Figure S3E and S7G). Therefore, a potential GSH peroxidase activity of Tsa1 is unlikely to contribute to the observed TIMDI formation and phenotypes.

Overall, peroxiredoxinylation occurs independent of hyperoxidized Tsa1 chaperone activity, with stress-induced TIMDI formation serving as a hallmark of redox-affected stresses and contributing to stress protection.

Identification of the redox-sensitive Tsa1 interactome in *S. cerevisiae*

Previously cysteine interactor traps were used to identify novel interactors for thioredoxins.[47,48] We employed the C171S mutant as an interactor trap to reveal TIMDI interactors without the need for stress induction. For a comprehensive understanding of the potential peroxiredoxinylation targets, we compared the redox-sensitive interactome of C171S and WT Tsa1 by mass spectrometry (Figure 4A). Performing a tandem affinity purification (TAP) of TAP-tagged WT and C171S mutant Tsa1 under reducing and NR conditions, we identified 211 interactors with $Tsa1^{WT}$-TAP and 599 with $Tsa1^{C171S}$-TAP by mass spectrometry (MS; Figure 4B; Data S1). Most of the binding partners showed redox-sensitive behavior and enrichment in NR conditions (Figures 4B and 4C). We found 43.6% of the $Tsa1^{WT}$-TAP interactors and 64.3% of the $Tsa1^{C171S}$-TAP interactors exclusively in the NR condition (NR-specific), supporting the idea of a redox-sensitive interactome of Tsa1. No particular consensus sequence or proximity of cysteines were indicators of interaction (Figure S4A and S4B). NR-specific interactors showed an overrepresentation with more than 5–8 cysteines, and only 1% lacked cysteines, which is 10 times fewer than expected from the overall proteome (Figure 4D; Data S2). Thus, general Tsa1-target interaction can be independent on (particular) cysteines, but redox-sensitive and covalent interactions are favored by the presence of cysteines. Binding of HSP70 (Ssa1 or Ssa2) is an example of a known non-covalent interaction with Tsa1, and accordingly, this interaction is found to be redox insensitive in our Tsa1 interactome (Data S1).[29]

There was >73% overlap between $Tsa1^{WT}$ and $Tsa1^{C171S}$ interactors, with C171S capturing a broader range, including less-expressed proteins (Figure 4E and S4E). A PANTHER overrepresentation test revealed carbohydrate metabolism, protein turnover processes such as translation, ribosomal biogenesis, chaperone function, and proteolysis to be overrepresented processes.[49] Additionally, metabolic processes such as amino acid biosynthesis, ATP generation, and glucose metabolism were significantly enriched (Figure 4F and S4C; Data S2). Supporting our findings, proteomics studies exploring cysteine accessibility and oxidations highlight cellular protein production and metabolism as oxidation sensitive processes[50,51] (Figure S4D). Proteins found in those processes generally are highly expressed, and most of

(G) Growth in ±1 mM sodium arsenite liquid medium. Optical density was measured every 10 min (n = 5). Median values ± SDs are shown.
(H) Arsenite-induced TIMDIs depends on Y78. Whole-cell extracts were prepared in NR conditions and separated by dual 10%/15% SDS-PAGE and analyzed by western blot.
(I) Cell fitness under arsenite stress depends on TIMDIs. Growth in liquid media ± 1 mM sodium arsenite. Optical density was measured every 10 min to follow (n = 5). Median values ± SDs are shown.
(A, C, D, E, and H) Glucose-6-phosphate dehydrogenase (G6PDH) was used as loading control.

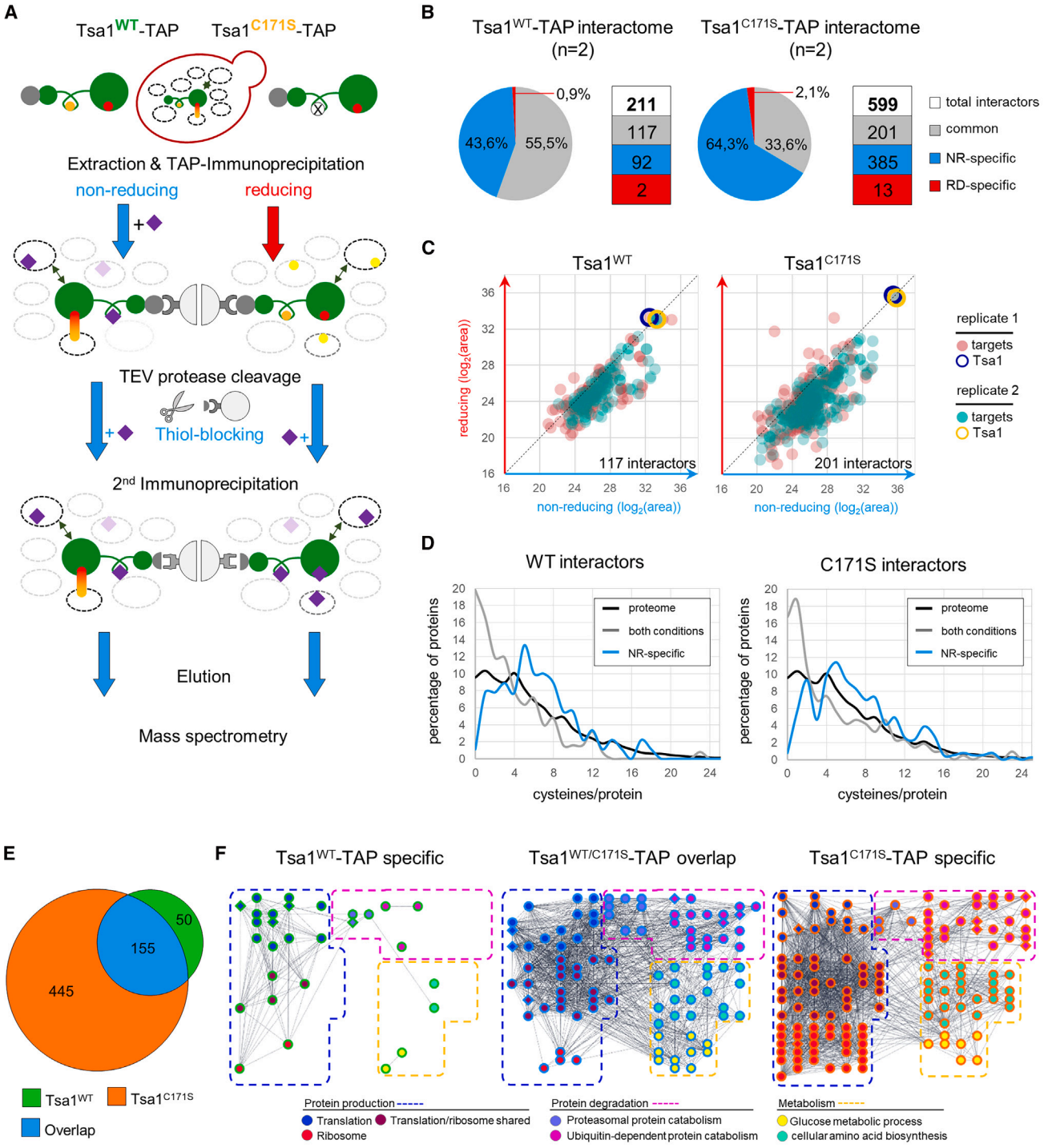

Figure 4. Tsa1 interacts with a large portion of the proteome in a redox-dependent manner

(A) Mass spectrometry (MS) workflow to identify the redox-sensitive interactome of Tsa1^{WT}-TAP and Tsa1^{C171S}-TAP. Depiction as in Figure 1A. Target cysteines (yellow-filled circles), C171S mutation (*x*), MMTS (S-Methyl methanethiosulfonate) (purple rhombus).

(B) Percentage of interactors that are found in NR and reducing conditions (common, gray) or are specific for one condition: NR (NR-specific, blue) and reducing (RD-specific, red). Absolute numbers of interactors are indicated.

(C) The $\log_2$ (area) values of Tsa1^{WT}-TAP and TSA1^{C171S}-TAP interactors were plotted as reducing (y axis) against NR (x axis). Binders detected in NR and reducing conditions (common) are represented. Tsa1 (hollow circles; blue = replicate 1, yellow = replicate 2), Interactors (filled circles; green = replicate 1, red = replicate 2). Numbers next to the x axis represent NR-specific interactors. Data are found in Data S1.

(legend continued on next page)

the interactors found belong to the 25% highest-expressed proteins (Figure S4E). The dynamic nature of TIMDIs might lead to an underestimation of Tsa1 targets. While the majority of Tsa1 targets—and Tsa1 itself—are highly expressed, the ability to form TIMDIs is not necessarily dependent on protein abundance. A 10-fold reduction of Tsa1 does not prevent TIMDI formation, but it does reduce the extent of TIMDIs upon oxidative stress (Figure S4F). Additionally, TDH3 having a CxxC motif and an abundance similar to that of Tsa1 does not show an extended MDI phenotype (Figure S4G). Thus, features of PRXs, such as high expression, cysteine oxidation sensitivity, and dual functions as peroxidase and chaperone, favor biological adduct formation.

In a complementary approach, we aimed to specifically enrich covalent and peroxidatic cysteine dependent interactors by DTT elution from a NR immunopurification of $Tsa1^{C171S}$-HA and $Tsa1^{C48S}$-HA strains (Figure 5A). Over two-thirds of proteins were eluted specifically from $Tsa1^{C171S}$ compared to $Tsa1^{C48S}$ (Figure 5B; Data S3). Common interactors between the mutants showed enrichment toward the resolving mutant, with 552 proteins identified as $Tsa1^{C171S}$ interactors (Figures 5B and 5C). A total of 60% of the cysteines were carbamidomethylated, indicating that they were in the thiol form in their native state. Close to 20% were *N*-ethylmaleimide modified (19.5%) or unmodified (20.4%) (Figure 5C). Consistent with findings from PRX-1 and -2 interactors, an enrichment for the CxxC motif in common $Tsa1^{C171S}$/$Tsa1^{C48S}$ eluted interactors was found (Figure S5A).[23] In contrast, C171S-specific interaction partners did not show this enrichment, indicating a different interaction mechanism. The number of cysteines/protein in the DTT-eluted interactors follow the trend observed for $Tsa1^{WT}$-TAP and $Tsa1^{C171S}$-TAP redox-sensitive interactors, with C171S interactors showing a slightly higher cysteine count per protein, but no correlation exists between cysteine linear distance or surrounding amino acid motifs (Figure 5D and S5B; Data S4). Almost half of the C171S DTT-eluted interactors were also found in the $Tsa1^{C171S}$-TAP interactome (Figure 5E). Likewise, a Gene Ontology analysis revealed that oxidative sensitive cellular processes related to protein production and carbohydrate metabolism were enriched (Figures 5F and S4). Supporting our MS approach, we found all Tsa1 redox interactors identified by Irokawa et al., namely Vma1, Cdc19/Pyk1, Ssb1/2,Frd1, and Yol057W.[52] Additionally, Hog1 and Bcy1, which have been shown to be covalently targeted by Tsa1, the PRX redox regulators Trx1/2 and Srx1, and proteins associated with Tsa1 (Ssa1/2 and Hsp104), have been identified here.[20,22,53,54] Together, the complementary MS approaches uncovered an extensive redox-sensitive interaction network of Tsa1 in the proteome.

Tsa1 associates with metabolic enzymes and regulates metabolism

Gluconeogenesis and the pentose phosphate (PP) pathway are affected in *tsa1Δtsa2Δ* double-deletion strains.[52] HMW forms of Tsa1 and Cdc19 were observed, but it was not known whether they associated covalently.[52] We asked whether the C48S and C171S point mutations in Tsa1 altered the metabolomic profile. We introduced both mutations into a completely auxotrophic FY4 strain and analyzed their metabolome by unbiased MS (Figure 6A, S6A, and S6B; Data S5). Changes were subtle and consistent with the largely unaffected growth of these mutants under standard conditions (Figure S6C). As expected from the disturbed redox balance of the Tsa1 mutants, the redox pair GSH and GSH disulfide (GSSG) were both increased. While the GSH:GSSG ratio is not significantly affected in the $Tsa1^{C48S}$ mutant, there was a clear decrease in the $Tsa1^{C171S}$ mutant, indicative of a more oxidizing environment.[55,56] This increased oxidative environment could contribute to the high TIMDI levels in the $Tsa1^{C171S}$ mutant. Consistent with previous reports, most upstream glucose metabolites increased in both mutants, while phosphoenolpyruvate decreased.[52]

Co-immunoprecipitation experiments with V5-tagged potential targets (Cdc19, Gnd1, Tdh3, Gpd1, Ugp1, and Eno2) confirmed their physical interaction with $Tsa1^{WT}$-HA and $Tsa1^{C171S}$-HA under reducing and NR conditions (Figure 6B). SDS-PAGE of whole-cell extracts revealed DTT-sensitive HMW adducts of these enzymes under NR conditions (Figure 6C, S6D, and S6E). A direct comparison of the Gnd1-V5 interaction with WT and C171S Tsa1 confirmed a stronger interaction of $Tsa1^{C171S}$-HA with Gnd1-V5 than $Tsa1^{WT}$-HA (Figure 6D). Similar to TIMDIs, HMW enzyme adducts were low under standard conditions but increased with stress (Figure S6F).

Co-immunoprecipitation (coIP) of WT and C171S Tsa1-HA with Cdc19-V5 or Gnd1-V5 confirmed that HMW adducts contained both Tsa1 and the metabolic enzymes (Figure 6E). Notably, the V5 tag did not affect survival or enzyme activity, and coIPs with Gnd1-V5 or untagged Cdc19 with endogenous Tsa1 yielded identical results (Figures S7A– S7F). Thus, the metabolic changes in Tsa1 mutants underscore its key role in regulating metabolic networks, aligning with Tsa1-interactome analyses.

Cys460 is an important residue for of Gnd1 function and is targeted by Tsa1

Gnd1 is a central enzyme of the oxidative branch of the PP pathway that has a strong redox-sensitive interaction with Tsa1 (Figures 6B–6E). The PP pathway fuels the cell with nicotinamide adenine dinucleotide phosphate, a key metabolite in redox reactions and oxidative stress protection.[57,58] Gnd1 forms more than a single HMW species in the $Tsa1^{C171S}$-HA background, indicating that more than one cysteine could be peroxiredoxinylated (Figures 6D and 6E). In contrast, in a Tsa1 WT strain, Gnd1 forms a single predominant HMW species induced by H_2O_2 (Figures 7A, 7D, and S8A). Covalent attachment of target cysteines to the peroxidatic cysteine of Tsa1 seems to prevent undirected mixed disulfide formation, judged by increased Gnd1 adducts in the $Tsa1^{C48S}$-HA mutant (Figure 7A and S8A). To understand this covalent interaction, we created a series of mutants in all cysteines of Gnd1. Some cysteine mutations reduced TIMDIs, while others

(D) Percentage of proteins (y axis) containing the indicated cysteine content/protein (x axis). NR and reducing conditions (common, gray), NR-specific (blue), and proteome-wide distribution (black). Due to the low number, reducing-specific candidates have been omitted from the analysis. Data are found in Data S2.
(E) $Tsa1^{WT}$-TAP (green) and $Tsa1^{C171S}$-TAP (orange) interactors overlap (blue). Interactor numbers are indicated in the sections.
(F) Representative Gene Ontology (GO) terms revealed by enrichment analysis. Full list, false discovery rate (FDR), and *p* values are found in Data S2.

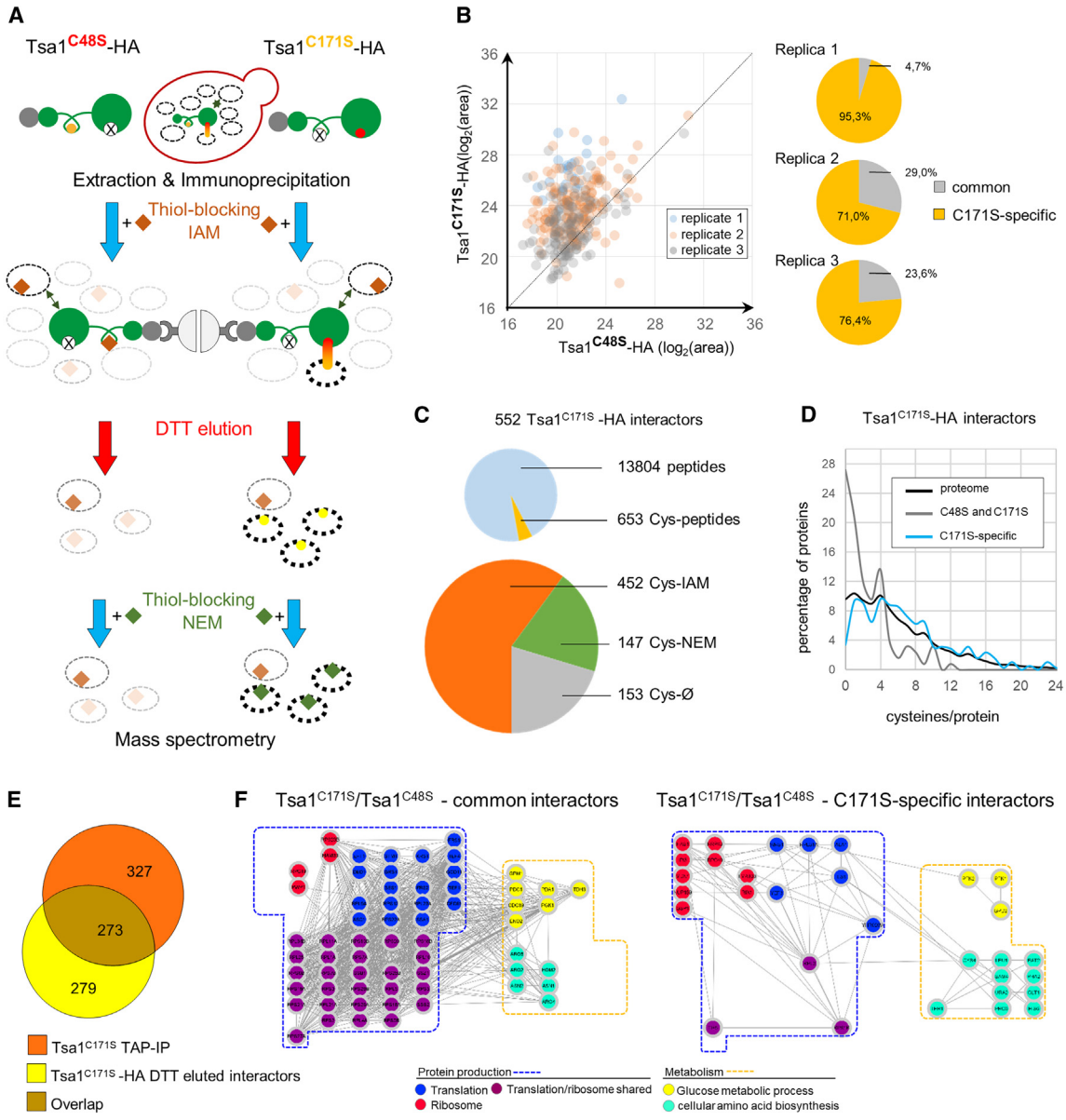

Figure 5. Sequential cysteine labeling identifies potential covalently associated targets to Tsa1

(A) MS workflow to identify redox-sensitive Tsa1^{C171S}-HA and Tsa1^{C48S}-HA interactors. Symbols are the same as were used in Figure 4A. C48S/C171S mutants (x), iodoacetamide (IAM) (brown rhombus), *N*-ethylmaleimide (green rhombus).

(B) DTT-eluted candidates identified in both mutants are plotted as Tsa1^{C171S}-HA versus Tsa1^{C48S}-HA (log_2 area values). Interactors identified in both Tsa1^{C171S}-HA and Tsa1^{C48S}-HA (common, gray) specific for Tsa1^{C171S}-HA (orange). Dataset can be found in Data S3.

(C) We identified 552 interactors in Tsa1^{C171S}-HA DTT-elutions in triplicate. Upper pie diagram shows the number of overall and cysteine-containing peptides. The lower pie diagram indicates the number of cysteines that are carbamidomethylated (Cys-IAM), *N*-ethylmaleimide modified (Cys-NEM), or unmodified (Cys-Ø). Absolute numbers are next to the pie charts.

(D) Percentage of proteins (y axis) containing the indicated cysteine content/protein (x axis). DTT-eluted interactors present both mutants (gray, C48S and C171S), C171S-specific (blue), and the proteome-wide distribution (black). Data are found in Data S4.

(E) Overlap (brown) of interactors identified in the Tsa1^{C171S}-TAP immunoprecipitations (orange, see Figure 4) and DTT-eluted Tsa1^{C171S}-HA interactors in this experiment (yellow). Numbers of the interactors are indicated within the sections.

(F) Representative GO terms revealed by enrichment analysis. Full list of enriched GO terms, FDR, and *p* values are found in Data S4.

caused a strong increase (Figure 7B and 7C). All HMW adducts of Gnd1 variants depended on Tsa1 and disappeared in a *tsa1Δ* deletion (Figure S8B). The Gnd1^{C460S} mutation in Tsa1^{WT}-HA and Tsa1^{C171S}-HA backgrounds abolished the prevailing Gnd1 HMW adduct, making C460 the primary cysteine targeted by Tsa1 (Figures 7B–7E). Consistently, C460 has been identified to

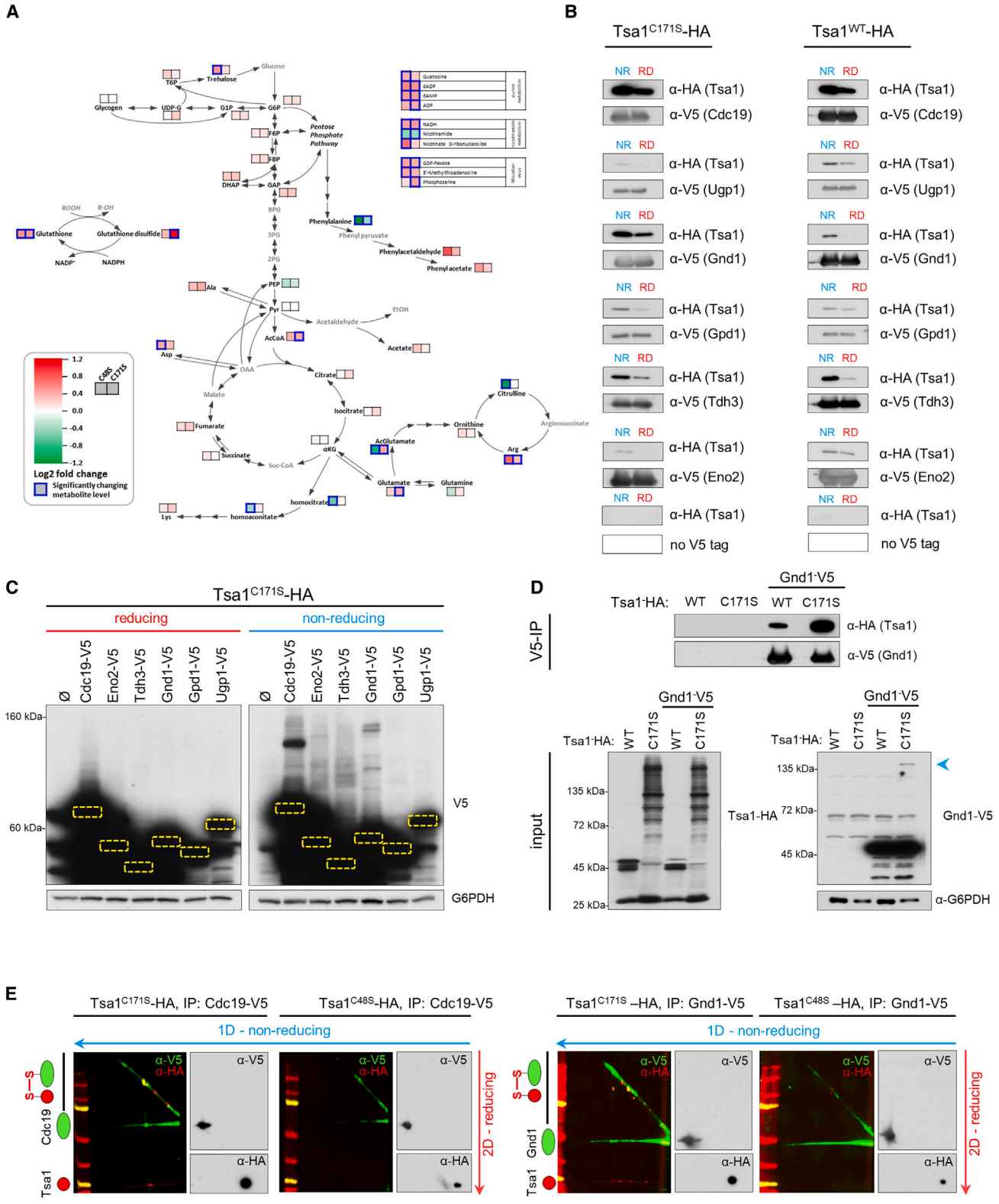

Figure 6. Tsa1 targets redox-sensitive metabolic enzymes

(A) Untargeted metabolomics reveals differences in glucose metabolism and the tricarboxylic acid cycle. Relative metabolite changes of C48S and C171S compared to the WT are shown. The dataset can be found in Data S5. Statistical analysis can be found in Figures S6A and S6B.

(legend continued on next page)

be surface exposed and thus accessible for covalent attachment to Tsa1.[51] Additionally, the loss of the predominant Gnd1-TIMDI species Gnd1^{C460S} increased MDIs of various sizes (Figures 7E and S8C).

The C terminus of Gnd1 is indispensable for its enzymatic activity, stabilizes the dimer, and forms a lid on the substrate-binding pocket.[59] Thus, C460 might be important for the catalytic activity of Gnd1. As expected, *gnd1Δ* cells have no detectable 6-Phosphogluconate dehydrogenase (6PDGH) activity (Figure S8D). In WT cells, a significant increase in 6PGDH activity was observed upon H_2O_2 stress, which was absent in the Gnd1^{C460S} mutant. Consistent with the role of Tsa1 in Gnd1 regulation, the TSA1^{C48S} mutant did not increase 6PDGH activity under H_2O_2 stress (Figure 7F). Thus, Gnd1 activity correlates with an increase in the Gnd1^{C460}- and Tsa1-dependent MDIs upon H_2O_2 stress (Figures 7D–7F, S8D, and S8E).

Analyzing growth, we found that WT cells recovered within 4–5 h upon H_2O_2 stress exposure, while *gnd1Δ*, Gnd1^{C460S}, and Tsa1^{C48S} cells are clearly delayed (Figure 7G). Similarly, under arsenite stress, 6PGDH activity was induced in WT cells but not in Gnd1^{C460S} and Tsa1^{C48S} mutants (Figure S8G). Correspondingly, cell growth recovery upon arsenite stress was delayed in Gnd1^{C460S}, gnd1Δ and Tsa1^{C48S} cells (Figure S8H) when compared to WT. Thus, we have identified C460 of Gnd1 as an important residue for phosphogluconate dehydrogenase activity by deciphering Gnd1 peroxiredoxinylation. This modification may protect Gnd1 from unwanted MDI formation, regulating activity during stress to ensure cell survival.

In contrast to Gnd1^{C460S}, the C365S mutant had strongly increased HMW adducts in a Tsa1^{C171S}-HA background (Figure 7B and 7C). Located at the A/B interface in the substrate-binding groove, we speculated that misfolding or enzymatic defects would lead to covalent attachment of Tsa1 as a quality control. To test this hypothesis, we selected isoleucine 366, which is not involved in substrate binding but resides in the binding groove next to C365 (Figure 7H) and mutated it to arginine or methionine. Indeed, Gnd1^{I366R} and Gnd1^{I366M} strongly affected 6PGDH activity (Figure 7I). Consistently, these mutants have increased Gnd1 HMW adducts that were abolished in the *tsa1Δ* deletion mutant (Figure 7J and S8F). Thus, while C460 of Gnd1 is targeted by peroxiredoxinylation to maintain enzymatic activity, mutations in residues critical for folding or catalytic activity could trigger Tsa1 attachment with a different outcome.

Thioredoxins regulate the extent of peroxiredoxinylation

Low basal TIMDI levels could be due to a redox environment that limits their formation or to negative regulation. The absence of a (structural) vicinal cysteine to C460 and the formation of MDI through multiple cysteine residues in Gnd1 mutants challenge the canonical redox relay as observed, for example, in Bcy1.[20,25] Could peroxiredoxinylation act as a recruiting signal for the protein folding machinery? In aged cells and oxidative stress, Tsa1-$SO_{2/3}$ binds to the Hsp70 chaperone and recruits Hsp104 to disaggregate protein aggregates, and oxidized Tsa1 is subsequently recycled via the sulfiredoxin Srx1.[29]

The deletion of Ssa1, Ssa2, and Hsp104 did not result in an altered TIMDI pattern (Figure S9A). In *srx1Δ*, the specific Srx1-Tsa1 adduct disappears upon oxidative stress, but general TIMDIs are unaffected (Figure S10A). Deleting thioredoxins (*trx1Δtrx2Δ*) resulted in a burst of TIMDIs (Figures S9A, S10A, and S10B). Additionally, TIMDI increases in the whole concentration range of H_2O_2 in *trx1Δtrx2Δ*, while peroxidatic hyperoxidation is strongly impaired, as observed in Tsa1^{C171S} (Figures S10C and S10D). We speculate that in the C171S mutant, Tsa1 oxidized dimers cannot form, so the sulfenic form reacts rapidly with cysteines on interactors. In *trx1Δtrx2Δ*, sulfenic Tsa1 partly forms TIMDIs and partly oxidizes to dimers (Figure S10A). Importantly, introducing a plasmid with the genomic region encoding *TRX1* or *TRX2* do partially rescue basal as well as 0.125-mM induced TIMDI formation (Figure S10E). Thus, both cytoplasmic thioredoxins resolve TIMDIs, and both genes must be functionally present. Additionally, the absence of thioredoxins led to strong mixed disulfide induction of Gnd1-V5, which was dependent on its C460 (Figure S9B).

Comparable to the C171S mutant, a more oxidizing environment likely contributes to high TIMDI levels in the *trx1Δtrx2Δ* mutant. In support of a direct, enzymatic targeting of thioredoxins in TIMDI resolution, we found that recombinant Trx1-HIS resolved general TIMDIs, as well as Gnd1-Tsa1 TIMDIs *in vitro* (Figure S9C). Furthermore, in *in vitro* assays, we detected only Tsa1-HA-Trx1-HIS adducts, indicating that TIMDIs are resolved by transferring the attached Tsa1 to Trx1 (Figure S10F). *In vivo* the Tsa1-Trx1 adduct would be subsequently resolved by an intramolecular disulfide formation in the thioredoxin, resulting in a reduced PRX and an oxidized thioredoxin, which subsequently can be resolved by the thioredoxin reductase system.[60] In conclusion, thioredoxins, not Hsp70/Hsp104, target Tsa1-MDIs for resolution.

DISCUSSION

PRXs are bifunctional enzymes that carry H_2O_2-detoxifying peroxidase and molecular chaperone functions, providing a framework for their diverse roles such as redox signaling.[17,61–63]

(B) V5-tagged metabolic enzymes were immunoprecipitated under reducing and NR conditions from Tsa1^{WT}-HA and Tsa1^{C171S}-HA strains. Corresponding blots of whole-cell extracts in (C) –(E).

(C) Western blot detection of V5-tagged enzymes from Tsa1^{C171S}-HA whole-cell lysates (corresponding to B). Monomeric enzymes (dashed yellow squares, shorter exposure in Figure S6E). G6PDH was used as loading control.

(D) Tsa1^{WT}-HA and Tsa1^{C171S}-HA strains ± Gnd1-V5 were used to immunoprecipitate (IP) Gnd1-V5 under NR conditions. V5-IPs and inputs were probed for anti-HA (Tsa1) and anti-V5 (Gnd1). Gnd1-V5 MDIs (blue arrowhead). G6PDH was used as loading control.

(E) The 2D-SDS-PAGE western blots of Cdc19-V5 and Gnd1-V5 immunoprecipitations. After separation in first dimension (NR, right to left) gel pieces were partially reduced and separated the second dimension (top down). Region of HMW adducts/TIMDIs was probed simultaneously with mouse anti-V5 (Gnd1-V5 or Cdc19-V5) and rabbit anti-HA (Tsa1-HA) and secondary fluorescence labeled antibodies. Membrane parts containing monomeric enzymes and Tsa1 were probed by the same primary antibodies and horseradish peroxidase secondary antibodies.

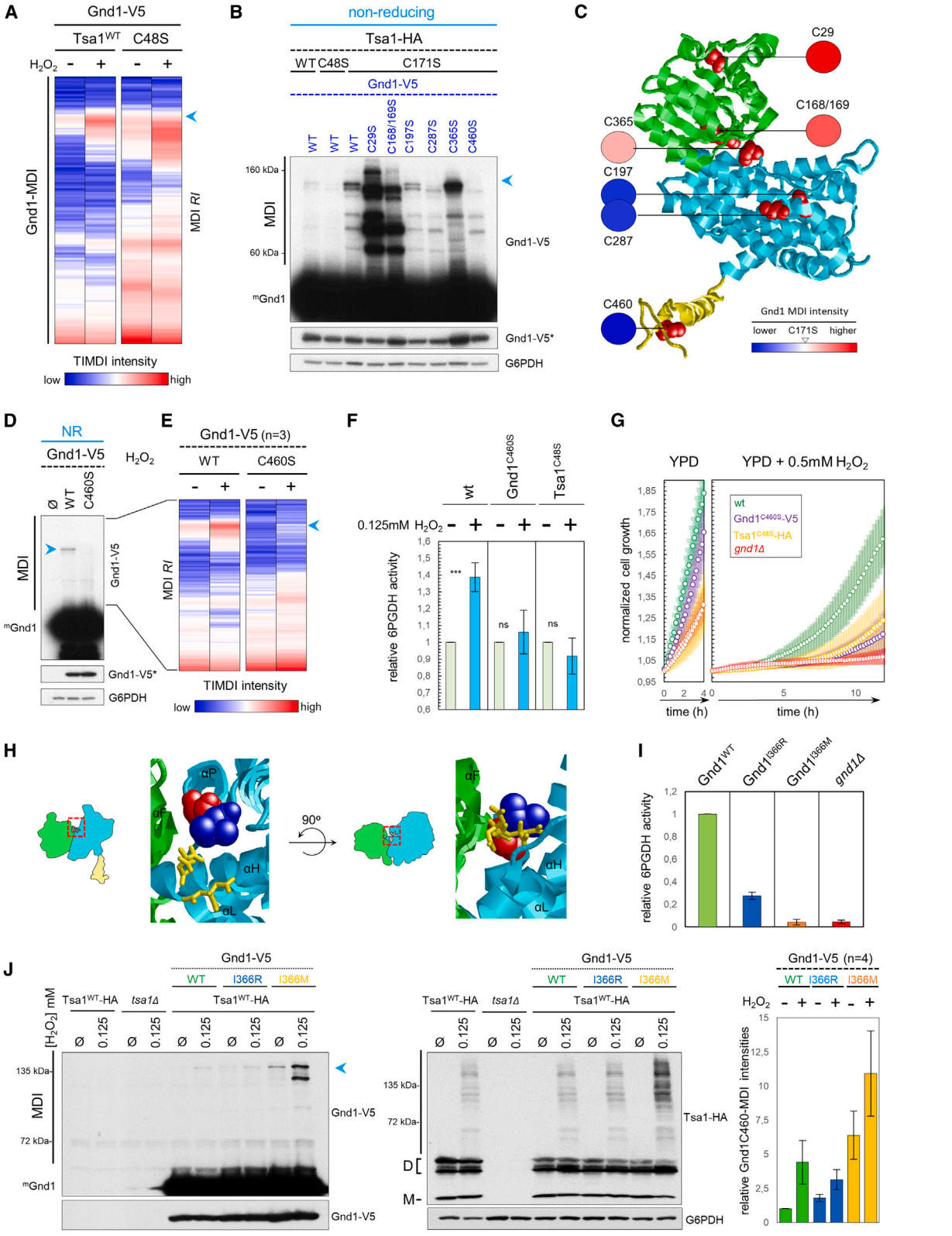

(legend on next page)

Studying *S. cerevisiae* PRX Tsa1, we found that it forms widespread Tsa1-induced MDIs, depending on the peroxidatic cysteine. Previously discovered MDIs in other organisms argue for an evolutionary conserved process.[23,24,64] About 20% of the discovered Tsa1 interactors correspond to cysteine-dependent interactors of human PRDX1 (Data S6).[23] Similar to Tsa1 interactors, human PRDX1 interactors are enriched for translation-related proteins. Comparison of PRX-redox-interactomes of various organisms will highlight which functions are conserved and which ones have changed in the course of evolution.

We observed that resolving cysteine mutants enhance TIMDI formation, showing that C_P-C_R disulfide exchange is not required for TIMDI formation. Upon H_2O_2 stress, a significant pool of Tsa1 is incorporated into TIMDIs. It will be interesting to decipher whether those targets are associated with recently discovered dynamic, localized redox microdomains.[65]

TIMDI formation does not require new protein synthesis or Hsp70/Hsp104-mediated protein disaggregation, two processes that Tsa1 has been implicated in, but rather targets mature proteins.[20,29] Additionally, deletion of the thioredoxins results in an increase of up to 60% of the Tsa1 pool in TIMDIs. While our results do not exclude that a change in the redox environment contributes to TIMDI formation in the Tsa1^{C171S} and thioredoxin deletion mutants, *in vitro* assays confirm that Tsa1^{C171S} can directly form TIMDIs with mature proteins, and thioredoxins are able to efficiently resolve TIMDIs *in vitro*.

In WT cells, various stresses induce TIMDIs that correlate with cycloheximide-resistant foci. It could be possible that target proteins and PRXs are concentrated in such foci, which triggers rapid TIMDI formation. Notably, the C171S mutant has a marked growth advantage over the WT and C48S Tsa1 in arsenite stress, indicating a protective role for TIMDIs. Moreover, impairing TIMDIs in the WT and the C171S Tsa1 renders cells sensitive to arsenite stress, reinforcing the link between TIMDI formation and stress protection.

Deciphering the redox-sensitive interactome of WT and Tsa1 C171S mutants revealed a redox-sensitive interactome with numerous proteins. The peroxidatic cysteine is crucial for many interactions, and peroxiredoxinylation appears widespread, involving proteins in key cellular processes like translation and metabolism. Evidence against TIMDI formation as an artifact includes significant overlap between interactors of WT and C171S mutant Tsa1 and confirmed interactions with glycolytic enzymes. While the resolving cysteine-to-serine mutation does not result in large structural changes, it exhibits a locally unfolded state that could favor covalent thiol attachment and hyperoxidation resistance, allowing MDI formation.[66] One hypothesis to be tested is that environmental conditions that lead to an increase in TIMDIs elicit a conformational state of WT Tsa1 that is at least partially equivalent to that of the C171S mutant.

Whether TIMDI formation follows the same mechanism and has a general stress-protective role in different stress conditions remains to be determined. In this study, we identified C460 in Gnd1 to associate covalently with the peroxidatic cysteine of Tsa1. This covalent association contributes to maintaining Gnd1 activity and survival upon oxidative and arsenite stresses.

Future studies are needed to decipher whether the protective function of TIMDIs is the sum of all covalent modification of Tsa1 targets or it relies on selected candidates. Identifying crucial cysteines like Gnd1^{C460} will be key to understanding stress-specific TIMDI mechanisms. For example, Cdc19 has been reported to interact in a redox-sensitive fashion with Tsa1, and we showed here that it is a candidate for a covalent disulfide link between Cdc19 and Tsa1. Generally, the interaction with various enzymes and the alteration of the metabolome indicate an important role in carbohydrate metabolism. While our metabolomics study does not allow us to draw conclusions on changes in fluxes, using Gnd1 (6PDGH), we clearly showed that Tsa1 targets this enzyme preferentially at a residue that is important for catalytic activity and important for survival upon oxidative stress.

Our model of PRX function proposes the following (the letters refer to those in Figure S9D): (A) in their peroxidase role, PRXs detoxify H_2O_2 from exogenous and endogenous sources. Thioredoxins resolve oxidized C_P-C_R dimers, maintaining the catalytic redox cycle. (B) Severe oxidative stress induces C48-hyperoxidized (SO_2/SO_3) chaperone formation, recruiting Hsp70/Hsp104 to refold aggregated proteins, followed by sulfiredoxin-mediated peroxidatic cysteine recovery.[17,29] (C and D) Upon stresses that affect the redox balance and folding of mature proteins, lead to an increased interaction of Tsa1 and

Figure 7. Gnd1^{C460}, a cysteine relevant for enzymatic activity and survival upon oxidative stress, is targeted by Tsa1

(A) Relative TIMDI intensities (*RI*) are shown as heatmaps (n = 3). Log_2-fold change and statistical analysis are in Figure S8A. Gnd1^{WT}-V5 MDI (arrowhead).

(B) Cysteine mutagenesis of Gnd1-V5 in the Tsa1^{C171S}-HA. Western blots of NR whole-cell extracts were probed with anti-V5 (asterisk denotes short exposure). Western blots for the same strains in a *tsa1Δ* can be found in Figure S8B. G6PDH was used as loading control. mGnd1, monomeric Gnd1-V5.

(C) Gnd1 crystal structure (PDB: 2P4Q): N-terminal A domain ($NADP^+$ binding, green), the central B domain (substrate binding, blue), and the C-terminal extension (lid formation, yellow). HMW adduct changes relative to the Gnd1^{WT}-V5 in the Tsa1^{C171S}-V5 background (circles).

(D) NR western blots of whole-cell extracts of WT and C460S Gnd1-V5 in the Tsa1^{WT}-HA background treated with 0.125 mM H_2O_2 for 10 min. G6PDH was used as loading control. mGnd1, monomeric Gnd1-V5.

(E) Relative TIMDI intensities (*RI*) are shown as heatmaps (n = 3). Log_2-fold change and statistical analysis are in Figure S8C. Gnd1-V5 MDI (arrowhead).

(F) Relative 6-gluconate dehydrogenase activity (n = 4). Median values ± SDs. Two-tailed Student's t test; ***$p < 0.0005$. H_2O_2 stress (0.125 mM, 40 min) values were normalized to the corresponding untreated sample (set to 1). *gnd1Δ* control is shown in Figure S8D.

(G) Growth curves in untreated (YPD medium, 4 h) and hydrogen peroxide conditions (YPD + 0.5 mM H_2O_2, 12 h).

(H) C365 (space fill red) and I366 (space fill blue) location at the Gnd1 domain A (green) and B (cyan) interface. Citrate molecules in the substrate binding pocket (yellow). Gnd1 crystal structure, PDB: 2P4Q. C365 (residue depicted as space filled model) and I366 (residue depicted as blue space filled model).

(I) I366 mutations reduce the Gnd1 6-phosphogluconate dehydrogenase (6PDGH) activity (n = 4). Median values ± SDs.

(J) Western blots of NR whole-cell extract of Gnd1 I366 mutants were probed for V5 (Gnd1) and HA (Tsa1) to visualize the respective HMW adducts. Quantification of the Gnd1-V5 MDI (arrowhead) in the right panel (n = 3). Median values ± SDs. G6PDH was used as loading control.

targets. In this condition, PRXs can form covalent adducts with accessible cysteines (peroxiredoxinylation).[23] (C and D). In canonical redox relays, a vicinal cysteine releases the PRX, leaving an oxidized redox regulator (C).[19,20] Independent of this disulfide exchange reaction, thioredoxins resolve PRX-MDIs, regenerating non-modified target thiols and forming a PRX-thioredoxin intermediate (D).

Peroxiredoxinylation does not need an enzymatic ligation system such as that seen for ubiquitin ligases or kinases (phosphorylation). High PRX expression not only makes them important H_2O_2 detoxifiers but also increases target interaction, taking account of a local concentration increase by foci formation upon stress. Peroxidatic cysteine properties allows the formation of sulfenic/sulfinic Tsa1 and target thiol covalent modification at low H_2O_2 concentrations and likely other stress conditions. Without TIMDI formation, random mixed disulfide protein crosslink can occur that is damaging to the cell.

Thus, PRXs could act as guardians of thiol reactivity, with peroxiredoxinylation emerging as a bona fide post-translational modification regulating protein MDIs. The large extent of peroxiredoxinylation that we observed in this study is therefore an indication that new, redox-sensitive mechanisms of PRXs are likely to be discovered in the future.

Limitations of the study

We reported a redox-sensitive interactome of the *S. cerevisiae* PRX Tsa1. Under normal conditions, Tsa1 interacts with a small number of proteins, but approximately 20% of the Tsa1 pool forms covalent mixed-disulfide intermediates upon stress. This does not exclude a role for Tsa1 under normal conditions but suggests a key role when protein damage increases upon stress. Furthermore, future studies are needed to address what fraction of the proteome is engaged in peroxiredoxinylation. We characterized Cys460 in Gnd1 (6PDGH) as an important residue for Tsa1-dependent regulation of enzymatic activity and survival. However, the detailed mechanism of the covalent interaction of Tsa1 to Gnd1 remains to be determined. Future studies are needed to define the role of Tsa1 in other biological processes and to identify important target cysteine residues in this context. Although we showed that TIMDI formation is required for proper cell survival upon arsenite stress, arsenite toxicity is pleiotropic, and the contribution of specific peroxiredoxinylation targets under this condition remains to be determined.

RESOURCE AVAILABILITY

Lead contact

Further information and material requests should be directed to and will be fulfilled by the lead contact, Francesc Posas (francesc.posas@irbbarcelona.org).

Materials availability

All unique reagents generated in this study are available from the lead contact with a completed materials transfer agreement.

Data and code availability

- Data: the raw proteomics data have been deposited to the PRIDE repository and are available via ProteomeXchange with identifier PXD034411. The raw metabolomics data have been deposited to the MetaboLights repository and are available with the identifier MTBLS11979.
- Code: this paper does not report any original code.
- Additional information: original data are available from the lead contact upon request.

ACKNOWLEDGMENTS

We thank Dr. P Latorre (IRB Barcelona) for help with the statistical analyses and C. Stephan-Otto Attolini and A. Caballe of the IRB Biostatistics Core Facility for their support with the statistical analysis of the data. We are grateful to Prof. Shusuke Kuge, Faculty of Pharmaceutical Sciences, Tohoku Medical and Pharmaceutical University, Sendai, Japan, for sharing antisera to detect endogenous Tsa1 and Cdc19. The laboratories of F.P. and E.d.N. are supported by a coordinated grant PID2021-124723NB-C21/C222 funded by MICIU/AEI/10.13039/501100011033 and ERDF/EU, and the Government of Catalonia (2017 SGR799). We gratefully acknowledge institutional funding from the Ministry of Science, Innovation, and Universities through the Centres of Excellence Severo Ochoa Award, and from the CERCA Programme of the Government of Catalonia and the Unidad de Excelencia María de Maeztu, funded by the AEI (CEX2018-000792-M). F.P. and E.d.N. are recipients of an ICREA Acadèmia award (Government of Catalonia). G.S. was supported by an Advanced Postdoc.Mobility fellowship (P300P3_147895) by the Swiss National Science Foundation.

AUTHOR CONTRIBUTIONS

G.S. and Z.R.N. performed the experiments; E.B. and E.S. performed the proteomic analysis; G.S., U.S., E.d.N., and F.P. participated in the design, data analysis, and writing of the manuscript.

DECLARATION OF INTERESTS

The authors declare no competing interests.

DECLARATION OF GENERATIVE AI AND AI-ASSISTED TECHNOLOGIES IN THE WRITING PROCESS

During the proofreading process, ChatGPT (OpenAI) was used. All proposed changes were reviewed and manually inserted into the text.

STAR★METHODS

Detailed methods are provided in the online version of this paper and include the following:

- KEY RESOURCES TABLE
- EXPERIMENTAL MODEL AND STUDY PARTICIPANT DETAILS
- METHOD DETAILS
  - Genetic manipulation of *S. cerevisiae*
  - Growth curves
  - Recombinant protein production
  - *In vitro* TIMDI resolution by thioredoxins
  - *In vitro* peroxiredoxinylation
  - Immunoprecipitations
  - Tandem affinity purification
  - Mass spectrometry
  - Immunoblotting
  - 2D SDS-PAGE
  - Image analysis
  - Metabolomics studies
  - 6-Phosphogluconate dehydrogenase activity measurements
  - Time lapse microscopy
  - Reagents and materials
- QUANTIFICATION AND STATISTICAL ANALYSIS

SUPPLEMENTAL INFORMATION

Supplemental information can be found online at https://doi.org/10.1016/j.celrep.2024.115224.

Received: October 5, 2022
Revised: August 13, 2024
Accepted: December 29, 2024

REFERENCES

1. Cecarini, V., Gee, J., Fioretti, E., Amici, M., Angeletti, M., Eleuteri, A.M., and Keller, J.N. (2007). Protein oxidation and cellular homeostasis: Emphasis on metabolism. Biochim. Biophys. Acta *1773*, 93–104. https://doi.org/10.1016/J.BBAMCR.2006.08.039.
2. Perkins, A., Poole, L.B., and Karplus, P.A. (2014). Tuning of Peroxiredoxin Catalysis for Various Physiological Roles. Biochemistry *53*, 7693–7705. https://doi.org/10.1021/bi5013222.
3. Peskin, A.V., and Winterbourne, C. (2020). Roles of 2-Cys Peroxiredoxins. Biochem. *86*, 84–91. https://doi.org/10.2210/pdb1QMV/pdb.
4. Radyuk, S.N., and Orr, W.C. (2018). The Multifaceted Impact of Peroxiredoxins on Aging and Disease. Antioxid. Redox Signal. *29*, 1293–1311. https://doi.org/10.1089/ars.2017.7452.
5. Hall, A., Nelson, K., Poole, L.B., and Karplus, P.A. (2011). Structure-based Insights into the Catalytic Power and Conformational Dexterity of Peroxiredoxins. Antioxid. Redox Signal. *15*, 795–815. https://doi.org/10.1089/ARS.2010.3624.
6. Davies, K.J. (1995). Oxidative stress: the paradox of aerobic life. Biochem. Soc. Symp. *61*, 1–31. https://doi.org/10.1042/BSS0610001.
7. Rhee, S.G., and Woo, H.A. (2010). Multiple Functions of Peroxiredoxins: Peroxidases, Sensors and Regulators of the Intracellular Messenger H 2 O 2 , and Protein Chaperones Introduction: From Thiol-Specific Antioxidant to Thioredoxin Peroxidase to Peroxiredoxin. Cell *140*, 454–456.
8. Rhee, S.G., Woo, H.A., Kil, I.S., and Bae, S.H. (2012). Peroxiredoxin Functions as a Peroxidase and a Regulator and Sensor of Local Peroxides. J. Biol. Chem. *287*, 4403–4410. https://doi.org/10.1074/JBC.R111.283432.
9. Chung, H.S., Wang, S.B., Venkatraman, V., Murray, C.I., and Van Eyk, J.E. (2013). Cysteine Oxidative Post-translational Modifications: Emerging Regulation in the Cardiovascular System. Circ. Res. *112*, 382–392. https://doi.org/10.1161/CIRCRESAHA.112.268680.
10. Módis, K., Ju, Y., Ahmad, A., Untereiner, A.A., Altaany, Z., Wu, L., Szabo, C., and Wang, R. (2016). S-Sulfhydration of ATP synthase by hydrogen sulfide stimulates mitochondrial bioenergetics. Pharmacol. Res. *113*, 116–124. https://doi.org/10.1016/J.PHRS.2016.08.023.
11. Sakai, J., Li, J., Subramanian, K.K., Mondal, S., Bajrami, B., Hattori, H., Jia, Y., Dickinson, B.C., Zhong, J., Ye, K., et al. (2012). Reactive oxygen species (ROS)-induced actin glutathionylation controls actin dynamics in neutrophils. Immunity *37*, 1037–1049. https://doi.org/10.1016/J.IMMUNI.2012.08.017.
12. Stojkov, D., Amini, P., Oberson, K., Sokollik, C., Duppenthaler, A., Simon, H.U., and Yousefi, S. (2017). ROS and glutathionylation balance cytoskeletal dynamics in neutrophil extracellular trap formation. J. Cell Biol. *216*, 4073–4090. https://doi.org/10.1083/JCB.201611168.
13. Grant, C.M., Quinn, K.A., and Dawes, I.W. (1999). Differential Protein S-Thiolation of Glyceraldehyde-3-Phosphate Dehydrogenase Isoenzymes Influences Sensitivity to Oxidative Stress. Mol. Cell Biol. *19*, 2650–2656. https://doi.org/10.1128/MCB.19.4.2650/ASSET/CF920DF7-02F7-43BA-9045-01233CFE9E35/ASSETS/GRAPHIC/MB0491547008.JPEG.
14. Wood, Z.A., Poole, L.B., and Karplus, P.A. (2003). Peroxiredoxin evolution and the regulation of hydrogen peroxide signaling. Science *300*, 650–653. https://doi.org/10.1126/SCIENCE.1080405/SUPPL_FILE/WOOD.SOM.PDF.
15. Klomsiri, C., Karplus, P.A., and Poole, L.B. (2011). Cysteine-based redox switches in enzymes. Antioxid. Redox Signal. *14*, 1065–1077. https://doi.org/10.1089/ARS.2010.3376.
16. Tachibana, T., Okazaki, S., Murayama, A., Naganuma, A., Nomoto, A., and Kuge, S. (2009). A Major Peroxiredoxin-induced Activation of Yap1 Transcription Factor Is Mediated by Reduction-sensitive Disulfide Bonds and Reveals a Low Level of Transcriptional Activation. J. Biol. Chem. *284*, 4464–4472. https://doi.org/10.1074/JBC.M807583200.
17. Jang, H.H., Lee, K.O., Chi, Y.H., Jung, B.G., Park, S.K., Park, J.H., Lee, J.R., Lee, S.S., Moon, J.C., Yun, J.W., et al. (2004). Two enzymes in one: Two yeast peroxiredoxins display oxidative stress-dependent switching from a peroxidase to a molecular chaperone function. Cell *117*, 625–635. https://doi.org/10.1016/j.cell.2004.05.002.
18. Barranco-Medina, S., Lázaro, J.J., and Dietz, K.J. (2009). The oligomeric conformation of peroxiredoxins links redox state to function. FEBS Lett. *583*, 1809–1816. https://doi.org/10.1016/J.FEBSLET.2009.05.029.
19. Sobotta, M.C., Liou, W., Stöcker, S., Talwar, D., Oehler, M., Ruppert, T., Scharf, A.N.D., and Dick, T.P. (2015). Peroxiredoxin-2 and STAT3 form a redox relay for H2O2 signaling. Nat. Chem. Biol. *11*, 64–70. https://doi.org/10.1038/NCHEMBIO.1695.
20. Kritsiligkou, P., Nowicki-Osuch, K., Carter, Z., Kershaw, C.J., Creamer, D.R., Weids, A.J., and Grant, C.M. (2021). Tolerance to nascent protein misfolding stress requires fine-tuning of the cAMP/PKA pathway. J. Biol. Chem. *296*, 100690. https://doi.org/10.1016/J.JBC.2021.100690.
21. Stöcker, S., Maurer, M., Ruppert, T., and Dick, T.P. (2018). A role for 2-Cys peroxiredoxins in facilitating cytosolic protein thiol oxidation. Nat. Chem. Biol. *14*, 148.
22. Cao, M., Day, A.M., Galler, M., Latimer, H.R., Byrne, D.P., Foy, T.W., Dwyer, E., Bennett, E., Palmer, J., Morgan, B.A., et al. (2023). A peroxiredoxin-P38 MAPK scaffold increases MAPK activity by MAP3K-independent mechanisms. Mol. Cell *83*, 3140–3154.e7. https://doi.org/10.1016/j.molcel.2023.07.018.
23. van Dam, L., Pagès-Gallego, M., Polderman, P.E., van Es, R.M., Burgering, B.M.T., Vos, H.R., and Dansen, T.B. (2021). The human 2-cys peroxiredoxins form widespread, cysteine-dependent-and isoform-specific protein-protein interactions. Antioxidants *10*, 627. https://doi.org/10.3390/antiox10040627.
24. Brandstaedter, C., Delahunty, C., Schipper, S., Rahlfs, S., Yates, J.R., and Becker, K. (2019). The interactome of 2-Cys peroxiredoxins in Plasmodium falciparum. Sci. Rep. *9*, 13542. https://doi.org/10.1038/s41598-019-49841-3.
25. Stöcker, S., Van Laer, K., Mijuskovic, A., and Dick, T.P. (2018). The Conundrum of Hydrogen Peroxide Signaling and the Emerging Role of Peroxiredoxins as Redox Relay Hubs. Antioxidants Redox Signal. *28*, 558–573. https://doi.org/10.1089/ARS.2017.7162.
26. Sideri, T.C., Stojanovski, K., Tuite, M.F., and Grant, C.M. (2010). Ribosome-associated peroxiredoxins suppress oxidative stress-induced de novo formation of the [PSI+] prion in yeast. Proc. Natl. Acad. Sci. USA *107*, 6394–6399. https://doi.org/10.1073/pnas.1000347107.
27. Noichri, Y., Palais, G., Ruby, V., D'Autreaux, B., Delaunay-Moisan, A., Nyström, T., Molin, M., and Toledano, M.B. (2015). In vivo parameters influencing 2-Cys Prx oligomerization: The role of enzyme sulfinylation. Redox Biol. *6*, 326–333. https://doi.org/10.1016/J.REDOX.2015.08.011.
28. Tairum, C.A., De Oliveira, M.A., Horta, B.B., Zara, F.J., and Netto, L.E.S. (2012). Disulfide biochemistry in 2-Cys peroxiredoxin: Requirement of Glu50 and Arg146 for the reduction of yeast Tsa1 by thioredoxin. J. Mol. Biol. *424*, 28–41. https://doi.org/10.1016/j.jmb.2012.09.008.
29. Hanzén, S., Vielfort, K., Yang, J., Roger, F., Andersson, V., Zamarbide-Forés, S., Andersson, R., Malm, L., Palais, G., Biteau, B., et al. (2016). Lifespan Control by Redox-Dependent Recruitment of Chaperones to Misfolded Proteins. Cell *166*, 140–151. https://doi.org/10.1016/J.CELL.2016.05.006.
30. Jarvis, R.M., Hughes, S.M., and Ledgerwood, E.C. (2012). Peroxiredoxin 1 functions as a signal peroxidase to receive, transduce, and transmit peroxide signals in mammalian cells. Free Radic. Biol. Med. *53*, 1522–1530. https://doi.org/10.1016/J.FREERADBIOMED.2012.08.001.
31. Marinho, H.S., Real, C., ısa Cyrne, L., Soares, H., and Antunes, F. (2014). Hydrogen peroxide sensing, signaling and regulation of transcription

factors. Redox Biol. *2*, 535–562. https://doi.org/10.1016/j.redox.2014.02.006.

32. Sousa-Lopes, A., Antunes, F., Cyrne, L., and Marinho, H.S. (2004). Decreased cellular permeability to H2O2 protects Saccharomyces cerevisiae cells in stationary phase against oxidative stress. FEBS Lett. *578*, 152–156. https://doi.org/10.1016/J.FEBSLET.2004.10.090.

33. Roger, F., Picazo, C., Reiter, W., Libiad, M., Asami, C., Hanzén, S., Gao, C., Lagniel, G., Welkenhuysen, N., Labarre, J., et al. (2020). Peroxiredoxin promotes longevity and H 2 O 2-resistance in yeast through redox-modulation of protein kinase A. Elife *9*, e60346. https://doi.org/10.7554/ELIFE.60346.

34. Martins, D., and English, A.M. (2014). Catalase activity is stimulated by H2O2 in rich culture medium and is required for H2O2 resistance and adaptation in yeast. Redox Biol. *2*, 308–313. https://doi.org/10.1016/J.REDOX.2013.12.019.

35. Sies, H., and Jones, D.P. (2020). Reactive oxygen species (ROS) as pleiotropic physiological signalling agents. Nat. Rev. Mol. Cell Biol. *21*, 363–383. https://doi.org/10.1038/S41580-020-0230-3.

36. Ho, B., Baryshnikova, A., and Brown, G.W. (2018). Unification of Protein Abundance Datasets Yields a Quantitative Saccharomyces cerevisiae Proteome. Cell Syst. *6*, 192–205.e3. https://doi.org/10.1016/J.CELS.2017.12.004.

37. Rand, J.D., and Grant, C.M. (2006). The thioredoxin system protects ribosomes against stress-induced aggregation. Mol. Biol. Cell *17*, 387–401.

38. Trotter, E.W., Rand, J.D., Vickerstaff, J., and Grant, C.M. (2008). The yeast Tsa1 peroxiredoxin is a ribosome-associated antioxidant. Biochem. J. *412*, 73–80. https://doi.org/10.1042/BJ20071634.

39. Weids, A.J., and Grant, C.M. (2014). The yeast peroxiredoxin Tsa1 protects against protein-aggregate-induced oxidative stress. J. Cell Sci. *127*, 1327–1335. https://doi.org/10.1242/jcs.144022.

40. Nadal-Ribelles, M., Solé, C., Xu, Z., Steinmetz, L.M., deNadal, E., and Posas, F. (2014). Control of Cdc28 CDK1 by a Stress-Induced lncRNA. Mol. Cell *53*, 549–561. https://doi.org/10.1016/j.molcel.2014.01.006.

41. Shalgi, R., Hurt, J.A., Krykbaeva, I., Taipale, M., Lindquist, S., and Burge, C.B. (2013). Widespread regulation of translation by elongation pausing in heat shock. Mol. Cell *49*, 439–452. https://doi.org/10.1016/J.MOLCEL.2012.11.028.

42. Rabdano, S.O., Izmailov, S.A., Luzik, D.A., Groves, A., Podkorytov, I.S., and Skrynnikov, N.R. (2017). Onset of disorder and protein aggregation due to oxidation-induced intermolecular disulfide bonds: case study of RRM2 domain from TDP-43. Sci. Rep. *7*, 11161. https://doi.org/10.1038/s41598-017-10574-w.

43. Jacobson, T., Navarrete, C., Sharma, S.K., Sideri, T.C., Ibstedt, S., Priya, S., Grant, C.M., Christen, P., Goloubinoff, P., and Tamás, M.J. (2012). Arsenite interferes with protein folding and triggers formation of protein aggregates in yeast. J. Cell Sci. *125*, 5073–5083. https://doi.org/10.1242/jcs.107029.

44. Oremland, R.S., and Stolz, J.F. (2003). The ecology of arsenic. Science *300*, 939–944. https://doi.org/10.1126/SCIENCE.1081903.

45. Loberg, M.A., Hurtig, J.E., Graff, A.H., Allan, K.M., Buchan, J.A., Spencer, M.K., Kelly, J.E., Clodfelter, J.E., Morano, K.A., Lowther, W.T., and West, J.D. (2019). Aromatic Residues at the Dimer-Dimer Interface in the Peroxiredoxin Tsa1 Facilitate Decamer Formation and Biological Function. Chem. Res. Toxicol. *32*, 474–483. https://doi.org/10.1021/ACS.CHEMRESTOX.8B00346.

46. Peskin, A.V., Pace, P.E., Behring, J.B., Paton, L.N., Soethoudt, M., Bachschmid, M.M., and Winterbourn, C.C. (2016). Glutathionylation of the active site cysteines of peroxiredoxin 2 and recycling by glutaredoxin. J. Biol. Chem. *291*, 3053–3062. https://doi.org/10.1074/jbc.M115.692798.

47. Ben-Lulu, S., Ziv, T., Admon, A., Weisman-Shomer, P., and Benhar, M. (2014). A substrate trapping approach identifies proteins regulated by reversible S-nitrosylation. Mol. Cell. Proteomics *13*, 2573–2583. https://doi.org/10.1074/MCP.M114.038166.

48. Benhar, M. (2017). Application of a Thioredoxin-Trapping Mutant for Analysis of the Cellular Nitrosoproteome. Methods Enzymol. *585*, 285–294. https://doi.org/10.1016/bs.mie.2016.09.003.

49. Thomas, P.D., Ebert, D., Muruganujan, A., Mushayahama, T., Albou, L.P., and Mi, H. (2022). PANTHER: Making genome-scale phylogenetics accessible to all. Protein Sci. *31*, 8–22. https://doi.org/10.1002/PRO.4218.

50. Brandes, N., Reichmann, D., Tienson, H., Leichert, L.I., and Jakob, U. (2011). Using Quantitative Redox Proteomics to Dissect the Yeast Redoxome. J. Biol. Chem. *286*, 41893–41903. https://doi.org/10.1074/JBC.M111.296236.

51. Marino, S.M., Li, Y., Fomenko, D.E., Agisheva, N., Cerny, R.L., and Gladyshev, V.N. (2010). Characterization of surface-exposed reactive cysteine residues in Saccharomyces cerevisiae. Biochemistry *49*, 7709–7721. https://doi.org/10.1021/bi100677a.

52. Irokawa, H., Tachibana, T., Watanabe, T., Matsuyama, Y., Motohashi, H., Ogasawara, A., Iwai, K., Naganuma, A., and Kuge, S. (2016). Redox-dependent Regulation of Gluconeogenesis by a Novel Mechanism Mediated by a Peroxidatic Cysteine of Peroxiredoxin. Sci. Rep. *6*, 33536.

53. Garrido, E.O., and Grant, C.M. (2002). Role of thioredoxins in the response of Saccharomyces cerevisiae to oxidative stress induced by hydroperoxides. Mol. Microbiol. *43*, 993–1003. https://doi.org/10.1046/J.1365-2958.2002.02795.X.

54. Molin, M., Yang, J., Hanzén, S., Toledano, M.B., Labarre, J., and Nyström, T. (2011). Life span extension and H(2)O(2) resistance elicited by caloric restriction require the peroxiredoxin Tsa1 in Saccharomyces cerevisiae. Mol. Cell *43*, 823–833. https://doi.org/10.1016/J.MOLCEL.2011.07.027.

55. Gostimskaya, I., and Grant, C.M. (2016). Yeast mitochondrial glutathione is an essential antioxidant with mitochondrial thioredoxin providing a back-up system. Free Radic. Biol. Med. *94*, 55–65. https://doi.org/10.1016/J.FREERADBIOMED.2016.02.015.

56. Jones, D.P. (2002). [11] Redox potential of GSH/GSSG couple: Assay and biological significance. In Methods in Enzymology (Academic Press), pp. 93–112. https://doi.org/10.1016/S0076-6879(02)48630-2.

57. Stincone, A., Prigione, A., Cramer, T., Wamelink, M.M.C., Campbell, K., Cheung, E., Olin-Sandoval, V., Grüning, N.M., Krüger, A., Tauqeer Alam, M., et al. (2015). The return of metabolism: Biochemistry and physiology of the pentose phosphate pathway. Biol. Rev. *90*, 927–963. https://doi.org/10.1111/brv.12140.

58. Ge, T., Yang, J., Zhou, S., Wang, Y., Li, Y., and Tong, X. (2020). The Role of the Pentose Phosphate Pathway in Diabetes and Cancer. Front. Endocrinol. *11*, 365. https://doi.org/10.3389/fendo.2020.00365.

59. He, W., Wang, Y., Liu, W., and Zhou, C.Z. (2007). Crystal structure of Saccharomyces cerevisiae 6-phosphogluconate dehydrogenase Gnd1. BMC Struct. Biol. *7*, 38. https://doi.org/10.1186/1472-6807-7-38.

60. Kim, J.A., Park, S., Kim, K., Rhee, S.G., and Kang, S.W. (2005). Activity assay of mammalian 2-cys peroxiredoxins using yeast thioredoxin reductase system. Anal. Biochem. *338*, 216–223. https://doi.org/10.1016/j.ab.2004.12.008.

61. Jung, C.L., Choi, H.I., Yu, S.P., Hyung, W.N., Hyun, A.W., Kwon, K.S., Yu, S.K., Sue, G.R., Kim, K., and Ho, Z.C.T. (2008). Irreversible Oxidation of the Active-site Cysteine of Peroxiredoxin to Cysteine Sulfonic Acid for Enhanced Molecular Chaperone Activity. J. Biol. Chem. *283*, 28873. https://doi.org/10.1074/JBC.M804087200.

62. Detienne, G., De Haes, W., Mergan, L., Edwards, S.L., Temmerman, L., and Van Bael, S. (2018). Beyond ROS clearance: Peroxiredoxins in stress signaling and aging. Ageing Res. Rev. *44*, 33–48. https://doi.org/10.1016/J.ARR.2018.03.005.

63. Kim, Y., and Jang, H.H. (2019). Role of Cytosolic 2-Cys Prx1 and Prx2 in redox signaling at MDPI AG. Antioxidants *8*, 169. https://doi.org/10.3390/antiox8060169.

64. Tiwari, S., Sharma, N., Sharma, G.P., and Mishra, N. (2021). Redox interactome in malaria parasite Plasmodium falciparum. Parasitol. Res. *120*, 423–434. https://doi.org/10.1007/s00436-021-07051-9.

65. Kritsiligkou, P., Bosch, K., Shen, T.K., Meurer, M., Knop, M., and Dick, T.P. (2023). Proteome-wide tagging with an H2O2 biosensor reveals highly localized and dynamic redox microenvironments. Proc. Natl. Acad. Sci. USA *120*, e2314043120. https://doi.org/10.1073/pnas.2314043120.

66. Peskin, A.V., Meotti, F.C., Kean, K.M., Göbl, C., Peixoto, A.S., Pace, P.E., Horne, C.R., Heath, S.G., Crowther, J.M., Dobson, R.C.J., et al. (2021). Modifying the resolving cysteine affects the structure and hydrogen peroxide reactivity of peroxiredoxin 2. J. Biol. Chem. *296*, 100494–100495. https://doi.org/10.1016/J.JBC.2021.100494.

67. Verduyn, C., Postma, E., Scheffers, W.A., and Van Dijken, J.P. (1992). Effect of benzoic acid on metabolic fluxes in yeasts: A continuous-culture study on the regulation of respiration and alcoholic fermentation. Yeast *8*, 501–517. https://doi.org/10.1002/YEA.320080703.

68. Huh, W.K., Falvo, J.V., Gerke, L.C., Carroll, A.S., Howson, R.W., Weissman, J.S., and O'Shea, E.K. (2003). Global analysis of protein localization in budding yeast. Nat *425*, 686–691. https://doi.org/10.1038/NATURE02026.

69. Ghaemmaghami, S., Huh, W.-K., Bower, K., Howson, R.W., Belle, A., Dephoure, N., O'Shea, E.K., and Weissman, J.S. (2003). Global analysis of protein expression in yeast. Nature *425*, 737–741. https://doi.org/10.1038/nature02046.

70. Gingras, A.C., Gstaiger, M., Raught, B., and Aebersold, R. (2007). Analysis of protein complexes using mass spectrometry. Nat. Rev. Mol. Cell Biol. *8*, 645–654. https://doi.org/10.1038/nrm2208.

71. Perkins, D.N., Pappin, D.J.C., Creasy, D.M., and Cottrell, J.S. (1999). Probability-based protein identification by searching sequence databases using mass spectrometry data. Electrophoresis *20*, 3551–3567.

72. Vizcaíno, J.A., Csordas, A., Del-Toro, N., Dianes, J.A., Griss, J., Lavidas, I., Mayer, G., Perez-Riverol, Y., Reisinger, F., Ternent, T., et al. (2016). 2016 update of the PRIDE database and its related tools. Nucleic Acids Res. *44*, D447–D456. https://doi.org/10.1093/NAR/GKV1145.

73. Schindelin, J., Arganda-Carreras, I., Frise, E., Kaynig, V., Longair, M., Pietzsch, T., Preibisch, S., Rueden, C., Saalfeld, S., Schmid, B., et al. (2012). Fiji: an open-source platform for biological-image analysis. Nat. Methods *9*, 676–682. https://doi.org/10.1038/NMETH.2019.

74. Raguz Nakic, Z., Seisenbacher, G., Posas, F., and Sauer, U. (2016). Untargeted metabolomics unravels functionalities of phosphorylation sites in saccharomyces cerevisiae. BMC Syst. Biol. *10*, 104. https://doi.org/10.1186/s12918-016-0350-8.

75. Ritchie, M.E., Phipson, B., Wu, D., Hu, Y., Law, C.W., Shi, W., and Smyth, G.K. (2015). limma powers differential expression analyses for RNA-sequencing and microarray studies. Nucleic Acids Res. *43*, e47. https://doi.org/10.1093/NAR/GKV007.

76. Sprouffske, K., and Wagner, A. (2016). SOFTWARE Open Access Growthcurver: an R package for obtaining interpretable metrics from microbial growth curves. BMC Bioinf. *17*, 172. https://doi.org/10.1186/s12859-016-1016-7.

77. Hothorn, T., Bretz, F., and Westfall, P. (2008). Simultaneous Inference in General Parametric Models. Biom. J. *50*, 346–363. https://doi.org/10.1002/BIMJ.200810425.

78. Lenth, R.V. (2016). Least-squares means: The R package lsmeans. J. Stat. Softw. *69*. https://doi.org/10.18637/jss.v069.i01.

STAR★METHODS

KEY RESOURCES TABLE

REAGENT or RESOURCE	SOURCE	IDENTIFIER
Antibodies		
mouse hybridoma αHA, clone 12CA5	NEB	P8108S
mouse monoclonal αV5	Invitrogen	R960-25; RRID: AB_2556564
anti-Peroxiredoxin-SO3	Abcam	ab16830; RRID: AB_443491
anti-Peroxiredoxin-SO2/3	Cambridge Research Biochemicals	crb2005004f
α-mouse IgG HRP-linked whole antibody	GE Healthcare	NA931; RRID: AB_772206
α-rabbit IgG whole antibody HRP	GE Healthcare	NA934; RRID: AB_772206
Rabbit polyclonal Tsa1	Gift from S. Kuge	N/A
Anti-6X His tag® antibody [HIS.H8]	Abcam	ab18184; RRID: AB_444306
Bacterial and virus strains		
N/A	N/A	N/A
Biological samples		
N/A	N/A	N/A
Chemicals, peptides, and recombinant proteins		
BamHI-HF	NEB	R3136S
NotI-HF	NEB	R3189S
NcoI-HF	NEB	R3193S
PreScission Protease	GE Healthcare	27-0843-01
endoproteinase LysC	Sigma-Aldrich	A0760
Trypsin	Wako	129–02541
digested bovine serum albumin	Promega	V5113
pre-stained molecular weight marker	AGFA	CPBU-NEW
Precision Plus Protein Dual Color marker	Sigma	SDS7B2-5X1VL
Expand High Fidelity Polymerase	Roche	11759078001
Glutathione Sepharose	Roche	17-0756-01
cOmplete™ His-Tag Purification Resin	Merck	5893682001
rabbit IgG-Agarose	Sigma	A2909
V5-Trap™ Magnetic Agarose	Chromotek	v5tma
L-Glutathione	Sigma	G4251
N-ethylmaleimide	Sigma-Aldrich	E3876
S-methyl methanethiosulfonate	Merck	64306
Iodoacetamide	Sigma	I1149
1,4-dithiothreitol	Sigma	D0632
Methanol, pure Ph Eur NF	Scharlab	ME0301005P
Tris Base	Sigma	T1378
Cycloheximide(100 mg/ml in DMSO)	Sigma	239765
L-azetidine-2-carboxylic acid	Thermo Scientific	C4859-1ML
30% Acrylamide:Bisacrylamide (37.5:1)	BioRad	161-0394SP
dNTPs (set of dATP/dCTP/dTP/dGTP)	Promega	U1420
IPTG	Roche	11411446001
Critical commercial assays		
Clarity Western ECL substrate	Bio-Rad Laboratories, S.A.	170–5061
6-Phosphogluconate Dehydrogenase Activity Colorimetric Assay	BioVision	K540

(*Continued on next page*)

Continued

REAGENT or RESOURCE	SOURCE	IDENTIFIER
Deposited data		
Proteomics data (PRIDE repository, EMBL-EBI)	This study	PXD034411
Metabolomics data (MetaboLights repository, EMBL-EBI)	This study	MTBLS11979
Experimental models: Cell lines		
N/A	N/A	N/A
Experimental models: *S. cerevisiae* strains		
MATa his3Δ1 leu2Δ0 met15Δ0 ura3Δ0 (BY4741)	ATCC	201388
BY4741 URA:pRSP5	This study	YGS338
BY4741 Tsa1 3' (URA)	This study	YGS347
Tsa1-GFP::HIS3	Yeast GFP Collection	YGS379
BY4741 *TSA1-1xHA::LEU*	This study	YGS447
BY4741 *TSA1^{C171S}-1xHA::LEU*	This study	YGS448
BY4741 *TSA1^{C48S}-1xHA::LEU*	This study	YGS449
BY4741 *TSA1-TAP::KAN*	This study	YGS456
BY4741 *TSA1^{C48S}-TAP::KAN*	This study	YGS457
BY4741 *TSA1^{C171S}-TAP::KAN*	This study	YGS458
FY4 Tsa1-1xHA::KanMX6	This study	YGS471
FY4 Tsa1^{C48S}-1xHA::KanMX6	This study	YGS472
FY4 Tsa1^{C171S}-1xHA::KanMX6	This study	YGS473
HSP104-GFP::HIS3;; TSA1-1xHA::LEU	This study	YGS836
YGS447 *GND1-1xV5:: HphNT1*	This study	YGS1026
YGS448 *GND1-1xV5:: HphNT1*	This study	YGS1028
YGS449 *GND1-1xV5:: HphNT1*	This study	YGS1030
YGS447 *hsp104::HIS3*	This study	YGS1053
YGS448 *CDC19-1xV5:: HphNT1*	This study	YGS1059
YGS447 *srx1::NatMX4*	This study	YGS1203
YGS448 *ENO2-1xV5:: HphNT1*	This study	YGS1267
YGS448 *UGP2-1xV5:: HphNT1*	This study	YGS1257
YGS448 *GPD1-1xV5:: HphNT1*	This study	YSG1271
YGS447 *ssa1::HphNT1 ssa2::NatMX4*	This study	YGS1275
YGS447 *trx1::KanMX6 trx2::NatMX4*	This study	YGS1313
YGS1026 *trx1::KanMX6 trx2::NatMX4*	This study	YGS1316
YGS447 *GND1^{C460S}-1xV5::HPH trx1::KanMX6 trx2::NatMX4*	This study	YGS1379
YGS447 *GND1^{C460S}-1xV5::HphNT1*	This study	YGS1541
YGS448 *GND1^{C29S}-1xV5:: HphNT1*	This study	YGS1551
YGS448 *GND1$^{C168/169S}$-1xV5:: HphNT1*	This study	YGS1552
YGS448 *GND1^{C197S}-1xV5:: HphNT1*	This study	YGS1553
YGS448 *GND1^{C287S}-1xV5:: HphNT1*	This study	YGS1554
YGS448 *GND1^{C365S}-1xV5:: HphNT1*	This study	YGS1555
YGS448 *GND1^{C460S}-1xV5:: HphNT1*	This study	YGS1557
YGS448 *TDH3-1xV5:: HphNT1*	This study	YGS1558
YGS447 URA:pRSP5>Tsa1	This study	YGS1573
BY4741 TDH3-1xHA::HphNT1	This study	YGS1733
YGS447 URA:pTDH3>Tsa1	This study	YGS1734
BY4741 URA:pTDH3	This study	YGS1735
Yeast GFP collection	Thermo Fisher Scientific	N/A

(*Continued on next page*)

Continued

REAGENT or RESOURCE	SOURCE	IDENTIFIER
Yeast TAP-tag collection	Horizon Discovery	N/A
Oligonucleotides		
see Table S1		
Recombinant DNA		
pGEX-6P-1	Sigma-Aldrich	GE28-9546-48
pGEX-6P-1-Tsa1C171S-HA	This study	pGS396
pRS413-gTRX1	This study	pGS558
pRS413-gTRX2	This study	pGS558
pETM10-TRX1	This study	pGS581
Software and algorithms		
FIJI	Fiji.sc	N/A
NIS elements AR	Nikon Instruments Inc.	N/A
Proteome Discoverer software suite (v1.4)	Thermo Fisher Scientific	N/A
Mascot search engine (v2.5)	Matrix Science	N/A
Other		
Centrifugal Filter Columns	Amicon	UFC901008
Transfer PVDF Immobilon-P, 0.45 μm	Millipore	IPVH00010
medical X-ray films (18 × 24 cm)	BioRad	1705060
LTQ-Orbitrap Velos Pro mass spectrometer	Thermo Fisher Scientific	N/A
EASY-nLC 1000	Thermo Fisher Scientific	N/A
Nikon Eclipse Ti	Nikon	N/A
ORCA digital camera	Hamamatsu	N/A
Agilent 6550 series quadrupole TOF MS	Agilent	N/A
GERSTEL MPS2 autosampler	Gerstel	N/A

EXPERIMENTAL MODEL AND STUDY PARTICIPANT DETAILS

Standard procedures were used for the growth and genetic manipulation of *Saccharomyces cerevisiae* (MATa his3Δ1 leu2Δ0 met15Δ0 ura3Δ0, S288C-derivative laboratory strain). Cells were grown at 30°C in YPD or in synthetic complete medium[67] with 2% glucose (metabolomics). GFP-tagged *S. cerevisiae* strains were obtained from the *ThermoFisher* Yeast GFP Clone Collection.[68] The Tsa1-TAP strains was obtained from the *Horizon* Yeast TAP Tagged ORFs Collection.[69] All *S. cerevisiae* strains generated or used in this study are listed in the key resources table.

METHOD DETAILS

Genetic manipulation of *S. cerevisiae*

For yeast transformation (deletion or knock in mutants using a PCR product as template for homologues recombination) a 50mL culture was grown to OD_{600} = 0.6–0.8. Cells were harvested by centrifuging at 3000 rpm for 3'. Cell pellet was washed with 500μL 10mM Tris-HCl, pH 8.0, supplemented with 1mM EDTA and 100mM Lithium acetate and centrifugation step was repeated. Pellet was re-suspended in 1mL of the same buffer. 100μL of cell suspension was added to a microfuge tube containing a mixture of 10μL 10 mg/ml heat denatured ssDNA with 1μg of PCR product and mixed well by flicking. 600μL of 40% PEG in 10 mM Tris-HCl, pH 8.0, with 1 mM EDTA and 100mM lithium acetate was added, tube was inverted five times and mix was incubated at 30°C for 45'. Then 70μL of DMSO was added, suspension was vortexed and heat shock at 45°C was applied for 15'. Cells were pelleted by centrifuging at 3000rpm for 1'. Pellet was resuspended in 400μL 10 mM Tris-HCl, pH 8.0 with 1 mM EDTA and was plated onto agar plates containing the auxotrophy selection medium. In case of antibiotic selection, cells were plated on YPD and replicated to antibiotic containing YPD plates using velvets 12h after transformation. The single C-terminally HA-tagged strains were generated by first inserting an auxotrophic marker 100bp 3′ of the Tsa1 stop codon in the endogenous locus in a BY4741 background to generate strain YGS347. Using genomic DNA from YGS347 as template PCR cassettes for homologous integration were amplified using *TSA1 mHA f01* (forward primer containing a single HA followed by a stop codon) and *Ctag TSA1 r03* (reverse primer) oligos. This cassette has been transformed into BY4741 to generate an endogenously single HA-tagged strain, YGS447. To generate endogenously single HA-tagged C171S (YGS448) and C48S (YGS449) mutants of Tsa1 cassettes for homologous recombination were amplified using

oligos *C171S wt f01* and *C48S f02*, respectively, and genomic YGS447 DNA as template. For single V5-tagging, the respective oligos found in Table S1 were used to generate PCR cassettes for homologous recombination using the pYM16 plasmid as template. To replace the promoter of Tsa1 with the promoter of Tdh3 or Rsp5 first an URA auxotrophic marker was inserted by homologous recombination in the 5′ genomic region of TDH3 (YGS1735) or RSP5 (YGS338). Genomic DNA from YGS1735/YGS338 was used as a template to generate a cassette to replace endogenous Tsa1 promoter of YGS447 strains.

Growth curves

S. cerevisiae strains were maintained in log-phase at least 12h before the experiment. For the experiment cells were diluted to OD_{600} = 0.1 and grown for 3h, then diluted to OD_{600} = 0.01 30′ before the start of the growth curve. Yeast cells were mixed with YPD or YPD containing stressors at 1:1 to a final volume of 200μL in 96-well plates. Plates were incubated under orbital shaking at 30°C in a Synergy H1 (BioTek Instruments) and OD_{600} was measured every 10'.

Recombinant protein production

$TSA1^{C171S}$ coding sequence was amplified from genomic YGS448 DNA (see key rescources table) and cloned into pGEX-6P-1 using BamHI-HF and NotI-HF. The resulting plasmid was transformed into BL21 and expression was induced using IPTG for 3 h. After purification using glutathione Sepharose, GST-tagged protein was eluted with L-glutathione. To remove L-glutathione buffer was exchanged to 50mM Tris_HCl, pH 7.0 supplemented with 150mM NaCl, 1mM EDTA, 1mM DTT, 0.01% NP40 using centrifugal filter columns. The GST-tag was removed by PreScission Protease. To this aim, 0.3μL of PreScission protease was added per 1μL buffer-exchanged recombinant protein and incubated at 12-16h. To the cleavage reaction 5x the volume of 50mM Tris-HCL pH8.0, 2mM DTT and 1.5x volume of the beads that were used for the initial GST-protein extraction was added and rotated for 1h at 4°C. Beads were removed by centrifugation and supernatant was concentrated using centrifugal filter columns.

TRX1 coding sequence was PCR-amplified from genomic BY4741 DNA and cloned into pETM10 using NcoI and NotI-HF. The resulting plasmid was transformed into BL21 and expression was induced using IPTG for 3 h. His-tagged Trx1 was purified on an Ni2+ Sepharose resin following the manufacturer's instructions (cOmplete His-Tag Purification Resin, Merck).

In vitro TIMDI resolution by thioredoxins

Gnd1-V5 or TSA1-HA were immunopurified from a *Δtrx1Δtrx2* mutant background using 10 mL culture of OD_{600} = 0.8 per condition under non-reducing conditions. All subsequent steps were conducted in an N_2 atmosphere: 2 μg of His-tagged Trx1 was added to beads suspended in reaction buffer (50 mM Tris-HCl, 1 mM EDTA, 150 mM NaCl, pH 7.5) and incubated at 30°C under shaking at 600 rpm. The reaction was stopped by adding the same volume of reaction buffer supplemented with 20 mM N-ethylmaleimide. Non-reducing sample buffer was added to a final concentration of 50mM Tris-HCl, 2% SDS, 10% glycerol, and 0.05% bromophenol blue. After samples were heated to 95°C for 2′ they were separated by SDS-PAGE and transferred to PVDF membranes.

In vitro peroxiredoxinylation

tsa1Δ cells were harvested at an OD_{600} = 0.5 and washed once in ice-cold 1xPBS, and whole-cell extracts were obtained by glass bead lysis in 50 mM Tris-HCl pH 8.0 and 2 mM DTT. For cysteine-blocked whole-cell extracts, 20mM N-ethylmaleimide was added to the buffer during extraction, followed by incubation for 30 min on ice, and buffer exchange to 50mM Tris-HCl pH 8.0 containing 2mM DTT was done using centrifugal filter columns. For the peroxiredoxinylation reaction, 400ng of whole cell extracts and 200ng of recombinant $Tsa1^{C171S}$ was mixed and dialyzed 3x against a 10kDa centrifugal filter column. After incubating the mix for 15 min at 30°C, the reaction was stopped by adding a double volume of 20mM iodoacetamide and dialyzing it two-times against a 10kDa centrifugal filter column at room temperature. Non-reducing sample loading buffer (final concentration of 50mM Tris-HCl, 2% SDS, 10% glycerol, and 0.05% bromophenol blue) was added to the samples, which were analyzed by immunoblotting.

Immunoprecipitations

Cells were harvested at OD600 = 0.6–0.8 and rapidly frozen in liquid N_2. Proteins were extracted by glass bead lysis in Buffer A (50mM Tris-HCl, 15mM EDTA, 15mM EGTA, 150mM NaCl, 0.1% Triton X-100 complemented with 1mM benzamidine, 1mM PMSF, 100μg leupeptin and 100μg pepstatin). N-ethylmaleimide, S-methyl methanethiosulfonate or iodoacetamide were used as thiol blocking agents at a concentration of 20mM during the lysis for non-reducing extraction. For reducing extraction 20 mM DTT was used. Lysates were diluted 1:10 with Buffer A and immunoprecipitation resin (beads) was added for 1 h on a rotating wheel at 4°C. After incubation with the sample, beads were washed by sequentially increasing the NaCl concentration (0.15/0.3/0.6/0.8 M) in Buffer A. For western blot analysis, beads were resuspended in sample loading buffer, boiled at 95°C for 2′ and loaded. Immunoprecipitation resin (beads) used in this study: rabbit IgG-Agarose (0.12μL slurry/ml of extract), V5-Trap Magnetic Agarose (0.24 μL/mL of extract), and HA-magnetic beads PierceTM (0.4 μL/mL of extract). All beads were blocked in BSA (5μL of 2 mg/ml stock in 1mL) supplemented 1xTBST for 30′ at 4°C. Before use, beads were equilibrated by washing 3x the beads with 500μL extraction buffer.

Tandem affinity purification

Strains for the tandem affinity purification are based on the Yeast TAP Tagged ORFs Collection.[69] 1000 mL of yeast culture ($OD_{60}0$ = 0.8) was harvested per replicate and frozen in liquid N_2. Subsequently, the pellet was resuspended in 24 mL of Buffer A and 4 mL of

resuspension was transferred to a 50-mL vial containing 2 mL of glass beads. Cells were lysed by vortexing 10 × 1 min with 1 min rest on ice between vortexing steps. Samples were cleared by centrifuging at 5000 rpm for 15 min (Allegra X-15R, Beckman-Coulter). Cleared lysates were pooled and 150μL of rabbit IgG-Agarose was added and incubated for 1h. Samples were further processed following the TAP purification protocol of the Gingras laboratory.[70]

Mass spectrometry

Sample preparation. Samples were digested with endoproteinase LysC (1:10 w:w, 37°C, ON), and trypsin (1:10 w:w, 37°C, 8h). After digestion, peptide mix was acidified with formic acid and desalted with a MicroSpin C18 column (The Nest Group, Inc) prior to LC-MS/MS analysis.

Chromatographic and mass spectrometric analysis. i) $TSA1^{WT}$ and $TSA1^{C171S}$ experiments. Samples were analyzed using an LTQ-Orbitrap Velos Pro mass spectrometer (Thermo Fisher Scientific, San Jose, CA, USA) coupled to an EASY-nLC 1000 (Thermo Fisher Scientific (Proxeon), Odense, Denmark). Peptides were loaded onto the 2-cm Nano Trap column with an inner diameter of 100 μm packed with C18 particles of 5 μm particle size (Thermo Fisher Scientific) and were separated by reversed-phase chromatography using a 25-cm column with an inner diameter of 75 μm, packed with 1.9 μm C18 particles (Nikkyo Technos Co., Ltd. Japan). Chromatographic gradients started at 93% buffer A and 7% buffer B with a flow rate of 250 nL/min for 5 min and gradually increased 65% buffer A and 35% buffer B in 60 min. After each analysis, the column was washed for 15 min with 10% buffer A and 90% buffer B. Buffer A: 0.1% formic acid in water. Buffer B: 0.1% formic acid in acetonitrile.

The mass spectrometer was operated in positive ionization mode with nanospray voltage set at 2.1 kV and source temperature at 300°C. Ultramark 1621 for the was used for external calibration of the FT mass analyzer prior the analyses, and an internal calibration was performed using the background polysiloxane ion signal at m/z 445.1200. The instrument was operated in data-dependent acquisition (DDA) mode and full MS scans with 1 micro scans at resolution of 60,000 were used over a mass range of m/z 350–2000 with detection in the Orbitrap. Auto gain control (AGC) was set to 1E6, dynamic exclusion (60 s) and charge state filtering disqualifying singly charged peptides was activated. In each cycle of DDA analysis, following each survey scan, the top twenty most intense ions with multiple charged ions above a threshold ion count of 5000 were selected for fragmentation. Fragment ion spectra were produced via collision-induced dissociation (CID) at normalized collision energy of 35% and they were acquired in the ion trap mass analyzer. AGC was set to 1E4, isolation window of 2.0 m/z, an activation time of 10 ms and a maximum injection time of 100 ms were used. All data were acquired with Xcalibur software. Digested bovine serum albumin was analyzed between each sample to avoid sample carryover and to assure stability of the instrument.

Acquired spectra were analyzed using the Proteome Discoverer software suite (v1.4, Thermo Fisher Scientific) and the Mascot search engine (v2.5, Matrix Science).[71] The data were searched against a Swiss-Prot yeast database plus a list of common contaminants and all the corresponding decoy entries. For peptide identification the precursor ion mass tolerance was set to 7 ppm, trypsin was chosen as enzyme and up to three missed cleavages were allowed. The fragment ion mass tolerance was set to 0.5 Da. Oxidation of methionine and N-terminal protein acetylation were used as variable modifications whereas dithiomethane was set as variable modification on cysteines. False discovery rate (FDR) in peptide identification was set to a maximum of 5%.

ii) Dual IAM-NEM experiments. Samples were analyzed using a Orbitrap Eclipse mass spectrometer (Thermo Fisher Scientific, San Jose, CA, USA) coupled to an EASY-nLC 1200 (Thermo Fisher Scientific (Proxeon), Odense, Denmark). Peptides were loaded directly onto the analytical column and were separated by reversed-phase chromatography using a 50-cm column with an inner diameter of 75 μm, packed with 2 μm C18 particles spectrometer (Thermo Scientific, San Jose, CA, USA).

Chromatographic gradients started at 95% buffer A and 5% buffer B with a flow rate of 300 nL/min and gradually increased to 25% buffer B and 75% A in 79 min and then to 40% buffer B and 60% A in 11 min. After each analysis, the column was washed for 10 min with 100% buffer B. Buffer A: 0.1% formic acid in water. Buffer B: 0.1% formic acid in 80% acetonitrile.

The mass spectrometer was operated in positive ionization mode with nanospray voltage set at 2.4 kV and source temperature at 305°C. The acquisition was performed in data-dependent adquisition (DDA) mode and full MS scans with 1 micro scans at resolution of 120,000 were used over a mass range of m/z 350–1400 with detection in the Orbitrap mass analyzer. Auto gain control (AGC) was set to 4E5 and injection time to 50ms. In each cycle of data-dependent acquisition analysis, following each survey scan, the most intense ions above a threshold ion count of 10000 were selected for fragmentation. The number of selected precursor ions for fragmentation was determined by the "Top Speed" acquisition algorithm and a dynamic exclusion of 60 s. Fragment ion spectra were produced via high-energy collision dissociation (HCD) at normalized collision energy of 28% and they were acquired in the ion trap mass analyzer. AGC was set to 1E5, and an isolation window of 1.4 m/z and a maximum injection time of 200 ms were used.

Digested bovine serum albumin was analyzed between each sample to avoid sample carryover and to assure stability of the instrument. Acquired spectra were analyzed using the Proteome Discoverer software suite (v2.0, Thermo Fisher Scientific) and the Mascot search engine (v2.6, Matrix Science). The data were searched against a Swiss-Prot Yeast database plus a list of common contaminants and all the corresponding decoy entries. For peptide identification a precursor ion mass tolerance of 7 ppm was used for MS1 level, trypsin was chosen as enzyme, and up to three missed cleavages were allowed. The fragment ion mass tolerance was set to 0.5 Da for MS2 spectra. Oxidation of methionine and N-terminal protein acetylation were used as variable modifications whereas carbamidomethylation and N-ethyl maleimide on cysteines was set as a fixed modification. False discovery rate (FDR) in peptide identification was set to a maximum of 5%.

The raw proteomics data have been deposited to the PRIDE repository with the dataset identifier PXD034411.[72]

Immunoblotting

Protein lysates for the evaluation of TIMDIs were prepared in lysis buffer (50 mM Tris-HCl, 2% SDS, 10% glycerol, and 0.05% bromophenol blue) containing 2 mM S-Methyl methanethiosulfonate or 2 mM 1,4-dithiothreitol. Proteins were separated by dual Tris-glycine SDS-PAGE (lower quarter 15%, upper $^{3}/_{4}$ 10% acrylamide gel and transferred to a P-type PVDF membrane using the BioRad wet transfer system. The following primary antibodies were used for western blotting: anti-HA (1:100), anti-V5 (1:2000), anti-G6PDH (1:10′000), and anti-Peroxiredoxin-$SO_{2/3}$ (1:2000). Since the polyclonal anti-Tsa1 antibody gives a more prominent background pattern and strains with untagged Tsa1 show a comparable TIMDI and peroxidatic hyperoxidation dynamics, we chose the tagged Tsa1 for western blot analysis (Figures S1C, S2C and S2D). Anti-mouse IgG HRP-linked whole antibody (1:10′000) and anti-rabbit IgG from donkey whole antibody HRP (1:10′000) were used as secondary antibodies. Membranes were imaged using the Clarity Western ECL substrate on medical X-ray films using an automated developing machine (Hyperprocessor, Amersham Pharmacia).

For infrared fluorescence detection using the LI-COR Odyssey Infrared Imaging System SDS-PAGE gel was transferred to an LF-type PVDF membrane and blocked with Intercept blocking buffer. Primary antibodies and secondary antibodies were also diluted in the same blocking buffer.

2D SDS-PAGE

For the 1st dimension, samples were separated on a 1-mm SDS-PAGE. The cut gel piece was incubated in 50 mM Tris-HCl 2% SDS with or without 5 mM DTT at 45°C for 10 min and rinsed in stacking gel mix before being placed horizontally on a 1.5-mm SDS-PAGE. The gel piece was overlaid with a stacking gel mix and electrophoresis was performed.

Image analysis

Films were scanned in TIF format at a resolution of 300 dpi using a (EPSON PERFECTION 4990 PHOTO, EPSON). Quantification for the TIMDI heatmap was done using the FIJI software.[73]

Metabolomics studies

Metabolite extraction, sample measurement and data processing for untargeted metabolomics was done according to.[74] In brief, strains were grown as quadruplicates in Verduyn media supplemented with 2 g/L glucose as carbon source in deep well plates. At OD595 0.60 ± 0.08, metabolites were extracted using a hot extraction protocol.

Ions within a mass/charge ratio range of 50–1000 were measured by direct flow double injection of extracts on an Agilent 6550 series quadrupole TOF MS with the aid of a GERSTEL MPS2 autosampler. Ion annotation was performed using the *S. cerevisiae* reactants defined in the KEGG database. All further analysis with ions corresponding to deprotonated metabolites was conducted using MATLAB (The Mathworks, Natick).

6-Phosphogluconate dehydrogenase activity measurements

Cells were grown to an OD600 = 0.5, and 1 mL/condition was harvested, washed once in 1xPBS and then frozen in liquid N_2 until processing. Sample extraction and 6-PGDH activity measurements were performed using the 6-Phosphogluconate Dehydrogenase Activity Colorimetric Assay Kit (BioVision, K540), following the manufacturer's protocol.

Time lapse microscopy

Cells were grown for 12h to reach an OD_{600} = 0.4 in low fluorescence media (YNB, CSM-URA supplemented with 2% glucose and 20 μg/ml uracil). 400μL of cells were seeded into 8 well microcopy chamber slide, previously coated with concanavalin A (1 mg/ml in dH_2O, wells were incubated with 300μL for 30′, washed twice with dH_2O and air dried). Cells were allowed to settle for 30′, supernatant was removed and 250ul low fluorescence media was added. Cycloheximide and/or AZC were added in 100μL media to achieve a final concentration of 100 μg/ml and 5mM, respectively.

Images were acquired at 60× magnification (Plan Apo VC 60× Oil objective) using a Nikon Eclipse T*i* inverted microscope and an ORCA digital camera (Hamamatsu) using the NIS elements AR software. CoolLED pE excitation system was used and GFP wide field fluorescence and bright field channels were used.

Reagents and materials

ssDNA oligos, reagents and materials used in this study can be found in the STAR Methods (key resource tables).

QUANTIFICATION AND STATISTICAL ANALYSIS

Data are shown as means with SD of at least three independent experiments. The number (n) of independent experiments is indicated in the figures.

Growth curves and enzyme kinetics were performed at least in triplicates (number of replicates is indicated in the figure, where n represents the number of biological replicates) and curves are depicted as median values ±standard deviation as indicated in the figure legends. In graphs of experiments with a replicate number of three, all data points are depicted in the figure.

Heatmap for relative TIMDI intensities was generated from western blots. To this aim, a linear selection starting at the highest molecular weight to the monomeric (in case of Gnd1) and dimeric (in case of Tsa1) protein form was used. Magnitude of intensity of pixels along this line was recorded. Experiments were performed in triplicates. From the same selection differential intensity analysis between stress conditions and the basal conditions was performed. Data was log normalized before fitting a linear model for each row, considering the experimental condition in the model. The ''lmFit'' function from the limma package was used to estimate the model coefficients, followed by the ''contrasts.fit'' function to consider the comparisons of interest and the ''eBayes'' function to estimate statistical significance.[75] P-value adjustment was done with the Benjamini-Hochberg method. Adjusted *p*-value lower than 0.05 was considered to for significant differences.

Growth curve parameters were estimated by fitting a logistic curve to the observed data of independent experiments using the function ''SummarizeGrowth'' of the growthcurver R package.[76] In order to compare conditions, a linear model was fitted to the parameters of the curves considering the experimental condition in the model. The ''glht'' function from the multcomp R package and confint function were used to estimate the coefficients and significance of the contrasts of interest.[77]

For enzyme activity curves comparison, background levels were subtracted from observed activity levels sample wise. Resulting values were further normalized by dividing by total protein levels. A linear model was fit to the normalized values including the combination of time and condition as covariate. The ''glht'' function was used to compare conditions at each time point. Furthermore, the slopes of the linear regime were estimated through a linear model including the interaction between the condition and the time variable. The experimental batch was also included to consider observed technical biases. An ANOVA analysis was performed to compare conditions. Finally, the ''lstrends'' function from the lsmeans R package was used to estimate the significance of the differences in slopes.[78] When applicable, batch adjusted values were computed by subtracting the corresponding coefficient estimated by the model.

In the metabolomics experiment, the ion-wise fold change was determined for each mutant against the wild type and a cutoff on the fold change was applied for removal of very small changes. For this purpose, the absolute log2 fold changes retrieved from replicate permutation of all wild-type ions were pooled, and the 99% quantile was determined to be at 0.3616. Accordingly, corresponding to a 30% change, the log2 fold change cutoff was defined at 0.3785. P-values were calculated by a two-sided 2-sample t test assuming unequal variance and corrected for multiple testing as previously described.[74] Ions with an absolute log2 fold change >0.3785 and a corrected *p*-value $<10^{-3}$ were considered significantly changing.